Joint Centre for Mesoscale Meteorology, Reading, UK

The Role of the Environmental Flow in the Development of Secondary Frontal Cyclones

A. J. Thorpe
I. A. Renfrew
C. H. Bishop

Internal Report No. 74

September 1997

Met Office Joint Centre for Mesoscale Meteorology Department of Meteorology
University of Reading PO Box 243 Reading RG6 6BB United Kingdom
Tel: +44 (0)118 931 8425 Fax: +44 (0)118 931 8791
www.metoffice.com

Designed and produced by the Met Office © Crown copyright 2001 01/0240 The Met Office logo is a registered trademark.

For submission to Quarterly Journal of the Royal Meteorological Society
First submitted 28th March 1996
Revised manuscript 2nd October 1996

The Role of the Environmental Flow in the Development of Secondary Frontal Cyclones

By Ian A Renfrew[1*], Alan J Thorpe[2] and Craig H Bishop[3]

[1]*Dept. of Physics, University of Toronto, Canada*
[2]*Dept. of Meteorology, University of Reading, UK*
[3]*Dept. of Meteorology, Pennsylvania State University, USA*

[*]Corresponding author: Department of Physics, University of Toronto, 60 St George Street, Toronto, Ontario, MS5 1A7, Canada.

SUMMARY

The impact of the environmental flow on the development of secondary frontal cyclones is investigated. Several case studies are examined as examples of secondary frontal cyclone events observed in the North Atlantic - Western Europe sector. A simple measure of growth is defined to chart their development. The vorticity attribution technique of Bishop (1996I&II) is utilised to calculate the action of the large scale (environmental) flow on the fronts. In particular the environmental along-front stretching - shown to be important in theoretical models of frontal instabilities - is calculated. The role of the environmental deformation appears to be crucial: as part of a baroclinic lifecycle, stretching deformation acts to build up a front but suppress along-front waves; if the stretching rate diminishes, barotropic instabilities may then break out. Diagnostics are examined to try to ascertain the growth mechanisms at work in each frontal cyclone case. A range of values for the commonly prescribed deformation frontogenesis and shearing frontogenesis parameters are calculated.

KEY WORDS

Secondary frontal cyclones, attribution, environmental flow, deformation.

1. INTRODUCTION

The downstream tail of the North Atlantic synoptic stormtrack appears to be the area most energetic in terms of sub-synoptic scale cyclonic activity (Ayrault *et al.* 1995). One subset of these sub-synoptic cyclones is that of secondary frontal cyclones, defined as waves on the pre-existing frontal zones of primary cyclonic systems. Such secondary frontal cyclones are an important and common local forecasting problem in western Europe, especially as they occasionally deepen explosively into full blown storms (eg. Hoskins and Berrisford 1988). Ordinary secondary frontal cyclones (those that do not deepen explosively) are typically up to 1000km in scale, fast growing and short lived (lifetimes of 1-2 days), see Hewson (1993) and Ayrault *et al.* (1995). Figure 1 shows one such frontal cyclone (L_{R1}) marked on the trailing cold front of a synoptic scale low system south of Greenland. This is an interesting case as two frontal cyclones develop, the one indicated and a second 12 hours later. The two cyclones appear similar in size and structure initially, but their evolutions are decidedly different - an explanation for this difference is put forward in section 3.

Theoretical modelling studies have found instabilities on the above lengthscales and timescales if the frontal zone includes a low level extremum in potential vorticity (Joly and Thorpe 1990, Malardel *et al.* 1993, Polavarapu and Peltier 1993); or equivalently a boundary potential temperature anomaly (Schär and Davies 1990, Joly 1995[1]). These situations are unstable to barotropic or internal baroclinic instabilities via the Charney-Stern (1962) instability criterion. The wave amplification can be thought of in terms of a phase locking and mutual amplification of edge waves on the edges of the potential vorticity strip or warm band (see for example Hoskins *et al.* 1985). However when the action of the environmental flow (ie. the baroclinic wave in which the front is embedded) is included, this is also found to be crucial to any frontal wave development. For example in Thorncroft and Hoskins (1990) the most unstable modes (about 1000km in scale) were torn apart when added to a baroclinic lifecycle experiment.

The two most important environmental flow mechanisms instrumental in forming and

---

[1]Note in Joly (1995) frontal waves were also found to amplify transiently, without a boundary potential temperature anomaly.

intensifying fronts are those of horizontal shearing and horizontal deformation. Several recent studies have examined the impact of these two frontogenesis mechanisms on the development of along-front waves. Joly and Thorpe (1991) investigated the growth of disturbances on a horizontal shearing forced front. For moist frontogenesis there was the possibility of rapid frontal cyclogenesis dependent upon two factors: the rate of frontogenesis and the state of the parent baroclinic wave. The authors suggest that the direct action of horizontal shearing deformation does not affect frontal wave growth; but indirectly larger shearing frontogenesis leads to a more potentially unstable front.

Bishop and Thorpe (1994I&II, hereafter *BT94I&II*) specifically investigated barotropic edge wave growth on an idealized moist tropospheric front in an external deformation flow. It was found that wave amplification depended upon the magnitude of the potential vorticity (PV) of the strip and the scale of the disturbance relative to the strip width. While the deformation flow and induced ageostrophic convergence act (via latent heat release) to increase the PV of the strip, they also tend to flatten nascent frontal waves. Furthermore the deformation frontogenesis process changes the non-dimensional wavelength of the waves through time - pushing them out of the 90° phase shift required for maximum amplification. Hence there is a trade off between keeping the waves in phase for as long as possible, and keeping the waves in phase when the PV of the strip is large and waves will amplify more rapidly. A stretching deformation rate of greater than $0.6\times10^{-5}s^{-1}$ suppresses most wave growth, at all scales; whereas a lower deformation rate of (for example) $0.2\times10^{-5}s^{-1}$ allows large amplification of frontal cyclone scale waves.

A highly idealized study by Dritschel *et al.* (1991) examined the role of external horizontal deformation and external horizontal shearing on edge wave growth. Of the two they found the suppressing action of the external deformation flow was the primary effect. The role of deformation on baroclinic instabilities is less clear cut - see Bishop (1993I&II).

It is clear from the above studies that both a potential for frontal instability and the evolving environmental flow are decisive in the development of any along-front waves. So for a proper analysis of observational data both the potential instability and the action of the environmental flow must be examined. The difficulty is that obtaining the relevant information from the complicated observational data is fraught with problems, for example the local structure

of the front masks the action of the environmental flow on the front. To compare the real atmosphere to theoretical models one really needs a way of partitioning the observed flow into separate parts - for example a *frontal* part and an *environmental* (background) part. This would allow a comparison between the front and its environment in the real atmosphere, and the front and its environment in a theoretical model. In other words such a partition would allow an analogy between the potential instability and its environment, and the perturbation and basic state parts of theoretical models. The two separate parts could then be analysed individually and relevant diagnostics calculated.

One way to achieve this partition is using an *attribution technique*, where an anomaly is isolated and a particular flow field is associated or attributed to that anomaly in some coherent manner. Utilising such a technique in a practical way has been the subject of recent research (eg. Hoskins *et al.* 1985, Davis and Emanuel 1991, Davis 1992, Bishop and Thorpe 1994a). The technique used in this study is that of domain independent vorticity and divergence attribution developed by Bishop (1996I&II). This technique is summarised in section 2. Using domain independent attribution allows the accurate calculation of the environmental stretching deformation rate shown to be crucial to frontal wave development in theoretical studies. In section 3 the relationship between frontal cyclone growth and the environmental stretching deformation is investigated for a variety of real case studies. Section 4 synthesizes the results of all the case studies, the aim being to provide a quantitative relationship between stretching deformation and frontal cyclone growth. Section 5 concludes the paper.

2. ANALYSIS TECHNIQUES

(a) Domain Independent Attribution

A horizontal wind field on a periodic or global domain can be uniquely partitioned[2] into *irrotational* and *nondivergent* parts (Helmholtz Theorem, see Morse and Feshbach 1953 for example). So for a horizontal wind $\boldsymbol{u}$,

$$\boldsymbol{u} = -\nabla\times(\psi\boldsymbol{k}) + \nabla\chi = \boldsymbol{u}_\psi + \boldsymbol{u}_\chi \qquad (1)$$

with streamfunction ψ and velocity potential χ, where $\boldsymbol{k}$ is the unit vector in the vertical. So $\boldsymbol{u}_\psi$ is nondivergent and $\boldsymbol{u}_\chi$ is irrotational. Defining the vertical component of the vorticity as $\xi = \boldsymbol{k}.\nabla\times\boldsymbol{u}$ and the divergence as $\delta = \nabla.\boldsymbol{u}$, then combining these and (1) leads to the Poisson equations:

$$\nabla^2\psi = \xi \quad \textit{and} \quad \nabla^2\chi = \delta \qquad (2)$$

So the nondivergent part of the wind $\boldsymbol{u}_\psi$ is due to the vorticity distribution, and the irrotational part of the wind $\boldsymbol{u}_\chi$ is due to the divergence distribution.

It is well known that such a unique partition is *not* possible on a finite domain, where the partition depends upon the boundary conditions imposed (eg. Lynch 1988, 1989). The approach of Bishop (1996I) bypasses this problem by solving the Poisson equations (2) using *free-space* Green's functions ie. where the boundary conditions are removed to infinity. This introduces a certain domain independence to the solutions. In 2 dimensions the Green's function is $ln(r)$, where r is the radial distance from the centre of the disc, so the induced winds are proportional to $1/r$.

---

[2]Note here the *partitioning* problem is that of separating a given wind field into irrotational and nondivergent parts as described for example in Lynch (1988). The word partition is also used in a more general sense elsewhere to mean the division of a wind field in some way. Closely related is the *reconstruction* problem which concerns the calculation of a wind field from given vorticity and divergence distributions (with winds given at the domain boundaries).

For discrete data in a finite domain, a unique wind field is attributed to each element of vorticity and divergence by calculating the wind field due to a disc of uniform vorticity and divergence assigned to each grid point in the domain. The vorticity and divergence of the discs are calculated via sophisticated circulation and flux estimates using wind data from the neighbouring grid points. To obtain the total *rotational* flow $\boldsymbol{u}_\psi$ (the flow due to all the vorticity in the finite domain) the wind induced by all the vorticity grid discs is summed. To obtain the total *divergent* flow $\boldsymbol{u}_\chi$ the wind induced by all the divergence grid discs is summed. As the domain is finite there is also a remainder flow: the *harmonic* part of the wind $\boldsymbol{u}_\upsilon$ defined by

$$\boldsymbol{u}_\upsilon = \boldsymbol{u} - \boldsymbol{u}_\psi - \boldsymbol{u}_\chi \qquad (3)$$

The harmonic wind is both solenoidal and irrotational in the domain, and so can be represented as a streamfunction ($\boldsymbol{u}_\upsilon = -\nabla\times\hat{\upsilon}\boldsymbol{k}$) or velocity potential ($\boldsymbol{u}_\upsilon = \nabla\hat{\upsilon}'$). It can be calculated independently by solving

$$\nabla^2\hat{\upsilon} = 0 \quad \textit{in the interior,} \quad \textit{subject to } \frac{\partial\hat{\upsilon}}{\partial n} = \boldsymbol{n}.\boldsymbol{u}_\upsilon \qquad (4)$$

where $\boldsymbol{n}.\boldsymbol{u}_\upsilon$ is calculated via (3) on the finite domain boundary. So the attribution technique allows a unique and unambiguous three component partition of the wind on a finite domain that is independent of the domain boundaries:

$$\boldsymbol{u}_{obs} = \boldsymbol{u}_\psi + \boldsymbol{u}_\chi + \boldsymbol{u}_\upsilon \qquad (5)$$

The rotational part of the wind is due to vorticity, the divergent part due to divergence, and the harmonic part due to vorticity and divergence outside the domain. Hence there is a clear relationship between a vorticity or divergence distribution and the wind field induced by it.

The details of the adaptation of the technique into a discrete formulation suitable for limited areas of gridded wind data is described in Bishop (1996I). Note the reconstruction of the wind field can be achieved to a high degree of accuracy: root-mean-square and maximum wind

errors are typically $0.1 ms^{-1}$ and $0.25 ms^{-1}$ respectively.

(b) Frontal Flow and Environmental Flow

The attribution method allows the association of a particular wind field to each grid point element of vorticity and divergence, so one can partition (or divide) a wind field by partitioning the vorticity and divergence distributions. In other words, one can specify a particular region of the domain and examine the flow due to vorticity and divergence in that region only. Following the ideas of Bishop (1996II) one can 'draw a box around' a cold front (Fig. 2) and define the *frontal* flow as the wind induced by vorticity and divergence inside the box, and the *external or environmental* flow as the wind induced by vorticity and divergence external to the frontal box (including vorticity and divergence outside the finite domain). Hence there is a division of the wind field into these two distinct parts:

$$\boldsymbol{u}_{obs} = \boldsymbol{u}_e + \boldsymbol{u}_i = \{\boldsymbol{u}_{e\psi} + \boldsymbol{u}_{e\chi} + \boldsymbol{u}_0\} + \{\boldsymbol{u}_{i\psi} + \boldsymbol{u}_{i\chi}\}, \qquad (6)$$

where $\boldsymbol{u}_e$ is the wind due to vorticity and divergence external to the frontal region (rotational + divergent + harmonic parts) and $\boldsymbol{u}_i$ is the wind due to vorticity and divergence inside the frontal region (rotational + divergent parts).

So to investigate the impact of the large scale flow on a front one would examine the environmental wind $\boldsymbol{u}_e$. This wind is due to vorticity and divergence distant from the front and so would be expected to be relatively smooth in the frontal region. It is this division into frontal and environmental flows that allows a comparison with theoretical model fronts and their division into perturbation parts and balanced basic states. In our partition the environmental wind ($\boldsymbol{u}_e$) is due to the synoptic system (and other surrounding systems) the front is embedded within, and the frontal wind ($\boldsymbol{u}_i$) is due to the front and any waves on the front. The prescribed *frontal box* may be defined as any shape: it is simply defined by the grid points that are inside the box (frontal) and those that are outside (environmental). In this study the frontal box is defined to enclose the strip of positive vorticity that typically delineates a baroclinic frontal zone, with the box edges

parallel to the strip. So for fronts and frontal waves the box used is either a rectangle or a segment of an annulus, thus covering both straight and curved fronts. At subsequent times the position of the frontal box is moved (and slightly elongated if necessary) so that the frontal wave is consistently enclosed.

To calculate the magnitude of the deformation flow shown to be crucial to modelled frontal wave development (Dritschel *et al.* 1991, *BT94II*), the along-front stretching due to the environmental flow is measured by $\partial v_e/\partial y_f$. Note there is a rotation of co-ordinates into a frontal co-ordinate system so (x_f, y_f) are the (across-front, along-front) directions respectively. The along-front direction is defined parallel to the frontal box sides, or as the arc through the centre of the frontal annulus. The across-front direction points towards the warm air for a cold front. Note for convenience the subscript *(f)* on the velocity is dropped and the subscript on the co-ordinate is retained.

As discussed in Bishop (1996II) if the stretching of the observed winds is used to estimate the deformation rate then serious errors may occur. Firstly the local structure of the front will cause along-front waves in the stretching pattern, and secondly a small variation in angle can cause a large change in stretching rate (due to the large shear associated with the front). Calculating stretching from the environmental winds dramatically reduces these errors, by 'removing' the frontal shear. A sensitivity study in Renfrew (1995), where the frontal box size and angle were varied by ±25% in width and ±3° in angle, found a variation of only 3% in $\partial v_e/\partial y_f$ from the prescribed deformation rate in an idealized front, and only $0.06\text{x}10^{-5}\text{s}^{-1}$ (10%) from the original box estimate in a real data case. This can be compared to variations of 15% and $0.25\text{x}10^{-5}\text{s}^{-1}$ respectively in calculating $\partial v_{obs}/\partial y_f$.

(c) A Measure of Frontal Wave Amplitude

A key issue is how to measure the size and growth of an observed frontal wave. Most analytical studies (eg. Dritschel *et al.* 1991, *BT94I&II*) use amplification of waveslope as a measure of growth, as it is proportional to the amount of nonlinear growth. Essentially the waveslope is the angle between an isoline of vorticity (for example) and its basic state position,

ie. on a horizontal plane $\partial\xi/\partial y_f$. Unfortunately defining and calculating waveslope in real data has a large error associated with it. To be measured the waveslope must be defined relative to some 'undisturbed' frontal position, and in observed fronts this undisturbed position is a conjectural matter. Ideally the measure of growth should be relatively insensitive to the chosen along-front direction. However as waveslope is defined relative to this direction it is intrinsically directly dependent upon it.

To overcome this problem a new measure of along-front variation has been developed starting from a practical, observational perspective rather than a theoretical one. The new measure of growth is the *peak vorticity* minus the *maximum along-front average vorticity* of the strip:

$$W(\xi) = \xi_{peak} - \max\{\overline{\xi}^{y}\} \qquad (7)$$

where y is the along-front direction. The peak vorticity is simply the maximum value in a specified frontal region (ie. the frontal box). To compare this peak value with the strength of the front, the along-front average vorticity for each column of grid points in the frontal box is calculated, and the maximum of these is subtracted from ξ_{peak} to obtain $W(\xi)$. We have called $W(\xi)$ the *vorticity wavyness*. The main advantages of $W(\xi)$ are that it is straightforward to calculate in observed flows, and does not depend directly on the along-front direction - only indirectly through the along-front average term. It appears from the real data sensitivity studies in Renfrew (1995) that $W(\xi)$ is relatively insensitive to small changes in the along-front direction - such changes give variations less than $0.06\times10^{-4}s^{-1}$ (8%) from the original box value. Vorticity wavyness is a simpler measure than waveslope, which means it should be less affected by small scale noise. However it is sensitive to model resolution (as are all vorticity measures) and to the length of the frontal region specified. Care needs to be taken that this vorticity strip length is defined consistently through the instability evolution - another reason for a 'Lagrangian' approach to defining the frontal box.

In Renfrew (1995) instabilities of a strip of vorticity in a numerical barotropic vorticity equation model are investigated, the results are similar to Dritschel *et al.* (1991). The amplitudes of the instabilities are measured using both waveslope and vorticity wavyness, and these

measures are shown to be comparable through the evolution of the frontal instability. This result provides some justification for the use of $W(\xi)$ on real data and interpreting the results in the context of other analytical work.

3. CASE STUDIES

A series of frontal cyclone case studies was investigated and the results are outlined below. A broad range of events was chosen and so each case exhibits distinctive features. However a detailed description of each case is beyond the scope of this paper and instead the reader is referred to Renfrew (1995). The key goals in the investigation are:

- measuring the growth of the frontal wave.
- examining the environment of the front in suppressing or allowing frontal wave growth.
- suggesting probable growth mechanisms on the basis of calculated diagnostics.
- measuring key parameters usually prescribed in frontal theory ie. the deformation rate α, and the horizontal shearing frontogenesis parameter s^2 (cf. Hoskins and Bretherton 1972).

The data used in this study are analyses from the UK Meteorological Office Unified Limited Area Model (LAM); this is described in detail in Cullen (1993) and references within. Analyses are processed four times daily at 00GMT, 06GMT, 12GMT and 18GMT, and note this is also local time for the UK in each case. The Unified Model (LAM version) is run operationally at a resolution of 0.44° latitude (approximately 50km grid resolution) with 19 vertical levels. Unfortunately the data are downgraded to 100km resolution for archiving purposes.

Clearly the analyses generated give only an incomplete representation of the atmosphere at any time. There will be processes occuring at sub-grid scales which will not be resolved by the model, and there will be errors in the resolved structures due to data collection errors and approximations made in the model formulation. Secondary frontal waves in the range 500-1000km in scale are towards the limit of what can be confidently represented in the LAM, especially in their development stage. Indeed it seems inevitable that there will be some errors

in data assimilation at various times and that these could cause inaccurate forecasts. This may have been the source of the poor forecast of 1st-2nd February 1994, see section (b). On the positive side, one recent innovation has been the routine assimilation of remotely sensed surface wind data over the oceans, determined via a scatterometer on the ERS-1 satellite (Bell 1994). This has improved data coverage over the otherwise data sparse Atlantic Ocean.

In each of the following cases the LAM analyses are taken as 'true' with some reservation given the above limitations. We are confident that the larger scale disturbances are well represented and that overall trends (growth and decay) of mesoscale systems are well represented, even if the precise details are not. So there is little doubt in our conclusions in each case, however some of the values of, for example, vorticity wavyness may not be exact. Note that the attribution calculation of environmental along-front stretching relies on the environmental winds being well represented. These are due mainly to the larger scale vorticity and divergence patterns, rather than the local structure, and this is well represented in general, so the environmental along-front stretching of the fronts will be accurately calculated.

(a) Case of 12th-13th November 1994

Figure 1 shows the mean-sea-level pressure analysis for 12GMT on the 12th November 1994, where a frontal cyclone (L_{R1}) is analysed with a weak pressure signature. A second frontal cyclone (L_{R2}) is subsequently analysed on the same frontal zone, southwest of the first. Initially the two frontal cyclones appear to have largely similar characteristics and be of similar horizontal size and depth. For example examination of the potential vorticity at 900mb shows the front defined by a PV strip approximately 0.4PVU greater than the surrounding area at 00GMT on the 12th (when the first frontal cyclone, L_{R1}, develops) and the same at 00GMT on the 13th when the second, L_{R2}, develops. Other diagnostics such as low level vorticity and temperature gradients also appear similar for the two waves. However the two frontal cyclones develop in markedly different ways. Over the 12th November L_{R1} increases rapidly in terms of vorticity wavyness $W(\xi)$ as seen in the vorticity plots (Figs. 3a&b) at 00GMT and 12GMT (12th) and graphed in Fig. 5. L_{R2} does not have such an increase in $W(\xi)$, but becomes less wavy and more 2 dimensional

through the 13th.

The hypothesis was that L_{R1} and L_{R2} were being affected in different ways by their environments. To calculate the environmental flow on the front a 'frontal box' was defined at each time and the external induced winds calculated (ie. those induced by vorticity and divergence external to the frontal box) as described in §2. The frontal boxes enclosing L_{R1} at 00GMT and 12GMT (12th), and enclosing L_{R1} and L_{R2} at 00GMT (13th) are outlined in bold in Fig. 3. Figure 4 shows contours of along-front stretching and wind vectors for the 00GMT frontal box: (a) for the observed winds $\boldsymbol{u}_{obs}$, and (b) for the environmental winds $\boldsymbol{u}_e$. Note there is a great deal of small scale structure in the $\partial v_{obs}/\partial y_f$ field even at this early time when L_{R1} is not that significant; the $\partial v_e/\partial y_f$ field is much smoother and more uniform giving an accurate representation of the background stretching deformation rate (the average over the central half of the box is $0.8\text{x}10^{-5}\text{s}^{-1}$). There are noticeable 'end effects' in the environmental stretching due to the cutting of the frontal vorticity strip (by the prescribed frontal box) causing extraneous circulations in the frontal region. By averaging over the centre of the domain their impact can be neglected, see Renfrew (1995) for a longer discussion.

The above analysis was carried out for the 30 hour period of investigation and the results are plotted in Figs. 5 and 6. Figure 5 shows vorticity wavyness $W(\xi)$ and the along-front averaged vorticity (a measure of frontal strength) and Fig. 6 shows the environmental stretching $\partial v_e/\partial y_f$ for both L_{R1} and L_{R2}. The vorticity wavyness of L_{R1} increases dramatically from 00GMT to 12GMT on the 12th, then drops off slowly as the frontal cyclone equilibrates. As shown in nonlinear frontal cyclone simulations (eg. Schär and Davies 1990, Malardel *et al.* 1993) if a frontal cyclone remains barotropic, the instability will quickly saturate and the wave will equilibrate. This appears to have happened for L_{R1} - it is not deep enough to move into a baroclinic growth phase. The rapid increase in $W(\xi)$ is coincident with a steady decrease in environmental along-front stretching of the front. The initially large $\partial v_e/\partial y_f$ average of $0.8\text{x}10^{-5}\text{s}^{-1}$ has halved to $0.4\text{x}10^{-5}\text{s}^{-1}$ by 12GMT and is negative by 00GMT on the 13th. In the idealized model of *BT94II*, sustained along-front stretching greater than $0.6\text{x}10^{-5}\text{s}^{-1}$ strongly inhibits frontal wave growth. The observed environmental stretching on L_{R1} falls below this value at about 06GMT. Over the following 6 hours, the vorticity wavyness $W(\xi)$ increases dramatically. Thus, in this case, the observations are

qualitatively and quantitatively consistent with their theoretical model. The data for L_{R1} concords with the hypothesis that a weakening environmental stretching rate allows the frontal wave to grow. The data for L_{R2} concords with the converse of this hypothesis - that is if the environmental stretching remains large (around $1x10^{-5}s^{-1}$ through to 06GMT on the 13th) then the frontal wave cannot develop.

To confirm this scenario along-front profiles of the environmental stretching were plotted; $\partial v_e/\partial y_f$ was calculated by averaging over the central few gridpoints of a longer frontal box enclosing both L_{R1} and L_{R2} at 00GMT (cf. Fig 3c) and 06GMT on the 13th. These show a geographical variation in the environmental stretching along the front - L_{R1} was in a low stretching regime (around $-0.2x10^{-5}s^{-1}$) and L_{R2} was in a high stretching regime (around $0.8x10^{-5}s^{-1}$) - the difference being due to their different locations relative to the synoptic systems. These different stretching regimes could certainly account for the different evolutions, indeed they concur with the barotropic edge wave modelling results of *BT94II*.

To check whether L_{R1} was growing through barotropic edge wave dynamics, derivatives of the perturbation wind field can be examined. The barotropic nature of frontal waves means that diagnostics such as pressure, streamfunction or temperature are swamped by the basic state (cf. *BT94II*, Fig. 8). Using the attribution method makes it possible to plot the observed wind equivalent of the theoretical perturbation wind derivatives. It should be noted that only the derivatives of the perturbation winds are compared. The partition of the observed wind field into frontal ($\boldsymbol{u}_f$) and environmental ($\boldsymbol{u}_e$) parts is (for practical reasons) not the same as the partition used in the theorertical studies of *BT94II*. The observed frontal winds ($\boldsymbol{u}_f = \boldsymbol{u}_{fg} + \boldsymbol{u}_{fx}$) include the frontal wave velocities and the frontal velocities, whereas in *BT94II* the perturbation winds are only the frontal wave velocities - the front is part of the basic state. However when taking along-front derivatives of $\boldsymbol{u}_f$ the frontal part is removed, as its along-front derivatives are zero, and so a comparison is valid. Figure 7 shows $\partial v_f/\partial y_f$ and $\partial u_f/\partial y_f$ for 12GMT and 18GMT on the 12th. Comparing the *v*-derivatives with Fig. 10 of *BT94II* the patterns are remarkably similar. The real data $\partial v_f/\partial y_f$ tilts with the shear and about 1½ wavelengths are coherent, there is other 'noise' but the comparison is reasonably convincing. Comparing the *u*-derivatives (with their Fig. 9) the patterns are less convincing. The cross-front wind is weaker and the derivative pattern is more

diffuse. At 12GMT $\partial u_t/\partial y_f$ is not that similar, but at 18GMT it is more like the theoretical pattern. It is likely that at the earlier time the signature of the weaker cross-front wind component is being masked by other noise; later on the cross-front flow is stronger and the pattern is more obvious. It does seem that barotropic processes are playing an important part in the development of L_{R1}.

Throughout the period the exterior induced horizontal shear $\partial v_e/\partial x_f$ is negative (ie. adverse to the shear of the vorticity front). It falls from around $-0.3\times10^{-5}s^{-1}$ at 00GMT on the 12th to about zero at 00GMT on the 13th (for the 900mb level). This decrease in environmental shear implies less suppression of barotropic instabilities (Dritschel 1989, Dritschel *et al.* 1991). However for the shears calculated here (and indeed in all the other tropospheric fronts investigated) this is very much a secondary factor.

In summary L_{R1} moved from an area of strong to weak environmental along-front stretching coincident with a period of rapid growth of the frontal cyclone. This increase in amplitude appears to be due to barotropic edge wave growth. In contrast L_{R2} remained in an area of strong environmental stretching and did not amplify, the growth mechanism was suppressed by the configuration of the synoptic systems. So the geographical distribution of stretching deformation was crucial in determining the different frontal cyclone evolutions.

(b) Case of 1st-2nd February 1994

At 18GMT on the 1st February 1994 (Fig. 8) a number of frontal cyclones are shown on a wavy cold front extending across Northern Europe and the North Atlantic. Two of these, L_Q and L_R, are shown with closed isobars and appear approximately the same size and magnitude. However their subsequent evolutions are totally different: L_Q remains an ordinary frontal cyclone - surface pressure staying around 1000mb before eventually saturating - whereas L_R deepens explosively (47mb in 42 hours) into a full blown storm. This is a particularly interesting case as the UK Met. Office 36 hour forecast was very poor - missing the explosive growth of L_R and instead deepening both L_Q and L_R to a moderate extent and with different locations (see Renfrew 1995).

It was hypothesised that the different evolutions of the two frontal cyclones may have

been due to different environmental flows. So the attribution technique was used to investigate the period from 00GMT on the 1st, to 12GMT on the 2nd February. On investigation it was found that both frontal cyclones were undergoing low stretching deformation through the 1st and 2nd (L_Q negative, around $-0.2\times10^{-5}s^{-1}$, and L_R positive, at $0\text{-}0.3\times10^{-5}\ s^{-1}$). These values are well below the critical mark of *BT94II* and so barotropic instabilities should be free to grow. Parker (1996) examines the effects of negative stretching on barotropic instabilities, and finds rapid but transient growth is possible. An examination of the Bishop (1993II) "f_1" case (for a mid-latitude baroclinic zone, cf. his Figs. 2 & 3) indicates this magnitude of strain also has a negligible effect on baroclinic growth. So the calculated environmental stretching should allow either (or both) L_Q and L_R to grow barotropically or baroclinically; so the action of the environmental flow does not seem to make the crucial difference in their developments.

The rapid deepening and increase in scale of L_R signifies a transition from a barotropic growth process to a baroclinic one, see Malardel *et al.* (1993). To grow baroclinically L_R must be large enough in scale to 'feel' the baroclinicity on the dynamical tropopause, ie. the horizontal scale must be larger than the Rossby radius (Malardel *et al.* 1993). A close examination of the size and depth of the two frontal cyclones, from pressure and vorticity diagnostics, reveals that L_R was marginally larger than L_Q. For example along-front cross-sections of potential vorticity (eg. at 12 GMT 2nd, Fig. 9) illustrate that L_Q was too shallow to phase lock with a tropopause undulation, whereas L_R was deep enough to phase lock with a more pronounced tropopause fold. Isentropic advection of PV from the stratosphere into the lower troposphere would thus allow a rapid deepening of L_R. This fits the scenario put forward by Thorncroft and Hoskins (1990) to explain the explosive growth of frontal cyclones: upper level reinforcement of a low level anomaly. Note although this explanation fits the available data, as discussed earlier the data are not perfect, and given the poor forecast, some caution must be expressed about the exact details of the growth mechanisms at work in this particular case.

The lack of large scale horizontal deformation motivates the comparison of this case with the horizontal shearing frontogenesis model of Joly and Thorpe (1991). Calculations of the *along-front* temperature gradient due to the large scale flow were made, via a 2 level balance approach - see the Appendix. It was found that the along-front temperature gradient was not that strong on

average. For example using the 900mb and 700mb levels, the along-front temperature gradient due to the environmental flow was about 0.1K/100km at L_R, and -0.2K/100km at L_Q, at 18GMT on the 1st. This would imply a small value of the s^2 parameter ($s^2 = g/\theta_0 . \partial\theta/\partial y_g$) for this time. In the Eady problem and in horizontal shearing frontogenesis models a typical value of s^2 is taken to correspond to an along-front gradient of ±0.5 to 1K/100km. The slow frontogenesis implied here would favour the amplification of 1000km-scale waves in the shearing frontogenesis model of Joly and Thorpe (1991). From these 1000km scale waves it seems one of them, L_R, becomes large enough to couple with a pronounced tropopause undulation and deepen explosively, whereas the other, L_Q, saturates through nonlinear processes.

(c) Case of 26th November 1994

This case was reminiscent of a classic Bergeron deformation forced front - the pressure analysis (Fig. 10) indicates a low level confluence flow on the front trailing southwards from L_L (954mb). The front was shallow but had a well defined signature in low level vorticity (Fig. 11), potential temperature and also in PV (magnitude 1PVU at 900mb). So instabilities of the type modelled in Joly and Thorpe (1990) or Schär and Davies (1990) would be possible. However the along-front stretching due to the environmental flow was calculated to be extremely strong: deformation rates between 1.2 & $1.6 \times 10^{-5} s^{-1}$ for the 900mb and 700mb u_e winds (00GMT to 12GMT). These are larger than the $1 \times 10^{-5} s^{-1}$ value usually prescribed in frontogenesis theory, and significantly greater than the critical values of *BT94II*.

From the *BT94II* model it is actually possible to calculate a minimum strain rate (α_{min}) necessary to suppress *all* barotropic frontal wave growth. For a valid comparison to be made it is necessary to check that the observed case and the idealisation are alike. So diagnostics of moist PV and relative humidity were examined to confirm that the front was close to moist neutrality ($PV_e \approx 0$) and saturated (the relative humidity was over 95%). Hence the following equation could be employed:

$$\alpha_{min} = \frac{f}{4}\left(\frac{\zeta_4 - \zeta_2}{\zeta_4 + \zeta_2}\right) e^{-2\mu} \qquad (8)$$

where ζ_4 is the absolute vorticity of the strip, ζ_2 is the absolute vorticity of the neighbouring anticyclonic region and 2μ is the nondimensional wavenumber of the disturbance. Taking $\zeta_4 = f + 1.0\text{x}10^{-4}\text{s}^{-1}$ and $\zeta_2 = f - 0.3\text{x}10^{-4}\text{s}^{-1}$ (Fig. 11) with $f = 1.0\text{x}10^{-4}\text{s}^{-1}$; then setting $2\mu = 0$ (ie. an infinite wavelength) sets an upper limit for α_{min}, so at 00GMT $\alpha_{min} = 1.2\text{x}10^{-5}\text{s}^{-1}$ for complete wave suppression. The measured value of $\partial v_e/\partial y_f$ is $1.6\text{x}10^{-5}\text{s}^{-1}$ so on this front the theory predicts that all waves should be suppressed. Note in reality 2μ is non-zero and instead the wavelength of any instability is limited by the width and length of the vorticity strip. An estimate of these at 00GMT gives a width of 250km and a length of 2500km, so $e^{-2\mu} = 0.63$ and $\alpha_{min} = 0.75\text{x}10^{-5}\text{s}^{-1}$ less than half the measured rate. However one must also consider that the magnitude of the vorticity of the frontal strip will not be fully resolved in the forecast model. If the relative vorticity of the strip is doubled ($\zeta_4 = f + 2.0\text{x}10^{-4}\text{s}^{-1}$), then α_{min} would be $0.98\text{x}10^{-5}\text{s}^{-1}$ for the estimated strip dimensions - also much less than the measured rate.

Over the next 12 hours the front remains fairly 2 dimensional, the vorticity wavyness $W(\xi)$ decreases from $0.7\text{x}10^{-4}\text{s}^{-1}$ at 00GMT to $0.3\text{x}10^{-4}\text{s}^{-1}$ at 12GMT, so as predicted wave growth is suppressed by the strong deformation flow.

(d) Case of 20th-22nd January 1995

A common scenario observed in the North Atlantic sector is when a mesoscale secondary cyclone 'runs around' the southern flank of a parent synoptic scale cyclone (the "Icelandic Low") and then deepens as it moves into the parent system, eventually becoming a parent cyclone itself (eg. Browning and Roberts 1994, Browning *et al.* 1995). This scenario occurred four times in succession in January 1995 and two of these events are investigated here.

Figure 12 shows a mean-sea-level pressure analyses at 18GMT on the 21st January: L_A has moved around L_S and is now a parent cyclone, with a col wave L_U growing on its front. L_A

shadowed an upper level PV tongue, and only deepened when the tongue moved over a low level baroclinic zone about 00GMT on the 21st. L_U was primarily a low level feature with a strong low level PV strip (1.2PVU at 00GMT on the 21st, see Renfrew 1995) but with the added complication of a meandering upper level tropopause anomaly (marked as a trough on Fig. 12) which also seemed to play a role in the low level growth.

Figure 13 shows the vorticity wavyness $W(\xi)$ and the along-front average vorticity over the period, for both L_A and L_U. There is an increase in $W(\xi)$ and along-front averaged vorticity for L_A around 00GMT on the 21st, coincident with the movement of the upper PV tongue over the low level baroclinic zone. Hence the growth process is envisaged as primarily a baroclinic interaction between the upper tongue and the low level baroclinicity, similar to that modelled in Thorncroft and Hoskins (1990). Initially there is not a strong enough low level PV strip at L_A for barotropic instabilities to play an important role. However the increase in amplitude of L_A does coincide with a decrease in environmental along-front stretching (Fig. 14) which would allow barotropic instabilities.

Turning to L_U, Fig. 13 illustrates the relative strength of the vorticity strip at L_U through the examination period. The frontal cyclone undergoes a rapid amplification from 06GMT to 12GMT (on the 21st) with a more gradual increase over a further 24 hours. The increase in $W(\xi)$ is coincident with a decrease in the environmental along-front stretching of L_U (Fig. 14). The amplification of L_U occurs when $\partial v_e/\partial y_f$ falls from $1.2\text{x}10^{-5}\text{s}^{-1}$ to around $0.8\text{x}10^{-5}\text{s}^{-1}$, this is towards the high end of the critical threshold zone for barotropic instabilities (cf. *BT94II*). What is striking, is the temporal change in stretching of L_U - there is a clear change from high to low stretching over 24 hours. This is also true for L_{RI} in case (a), see Fig. 6, and suggests that as well as the actual strain rate, the time rate-of-change of strain may also important. An extension of the *BT94II* model could be used to investigate this idea.

To investigate whether L_U was growing through barotropic processes the perturbation wind derivatives $\partial v_i/\partial y_f$ and $\partial u_i/\partial y_f$ were examined (as described for case (a) - Fig. 7). These showed the tilts with, and against, the vorticity strip shear that are indicative of barotropic growth, however the patterns were not as distinct as those in case (a). To ascertain whether baroclinic growth processes were present cross-sections of PV along the front were examined (as described

for case (b) - Fig. 9), and an along-front ('westerly') tilt with height was visible between the low level L_U and the upper level tropopause anomaly. However the magnitude of the tilting PV anomaly was not that great (0.8PVU). Note the low level PV strip had a maximum in the interior of the troposphere, around 1-2km in height, and so internal baroclinic growth may also be occurring (cf. Charney and Stern 1962). It is not certain which of the above growth mechanisms were the most important for the amplification of L_U, and a more comprehensive examination is beyond the scope of this study. However there is evidence of some barotropic edge wave growth, which the drop in environmental stretching allowed to occur.

4. DISCUSSION

To try and synthesize all the case study analyses into an overall picture, a regime diagram has been developed. Figure 15 plots the rate of change of vorticity wavyness $(dW(\xi)/dt)$ against environmental along-front stretching $(\partial v_g/\partial y_g)$ for all the cases investigated. The rate of change of $W(\xi)$ is a measure of the *growth* of a frontal cyclone. The along-front stretching rates are normalised by α_{min}, the minimum strain rate required to suppress all barotropic frontal wave growth (cf. Eq. 8 and *BT94II*). This normalisation accounts for the differing strengths of the vorticity strips in each case; clearly if the vorticity strip were not that anomalous then significant wave amplification through edge wave dynamics could not be expected.

The regime diagram allows the testing of a hypothesis suggested by the theoretical modelling work of Dritschel *et al.* (1991), *BT94II* and Renfrew (1995). The hypothesis is that *sustained strong along-front stretching is a sufficient condition for barotropic frontal stability; weak along-front stretching is a necessary condition for barotropic frontal instability.* To test the hypothesis all the points from all the cases are plotted, except those points where the frontal cyclone has started to saturate through nonlinear processes (ie. where the cyclone has left the developing stage, cf. Schär and Davies 1990, Malardel *et al.* 1993). This is judged to have happened if *(i)* the frontal cyclone has reached a finite amplitude size (defined by $W(\xi)$ greater than $1.0\times10^{-4}s^{-1}$); and *(ii)* the frontal cyclone is at the end of its lifecycle ($W(\xi)$ is monotonically decreasing). This eliminates 9 data points, leaving 20 points. The error bars indicate the

maximum variation found in the sensitivity study of Renfrew (1995), where the frontal box size and angle were varied by small amounts (see section 2). Note the rate of change of $W(\xi)$ is calculated by differencing the 6 hourly sampled values (ie. by differentiating the curves plotted in Figs. 5 and 13 for example). The corresponding $\partial v_e / \partial y_f$ is taken as the mean of the two stretching values of those times, normalised by α_{min}. The α_{min} is calculated for each time, with $2\mu=0$ (ie. infinite wavelength); recall this provides an upper bound for α_{min}. This means the *critical threshold* for barotropic wave suppression is a normalised stretching rate of 1; *weak* stretching is less than 1, and *strong* stretching is greater than 1. To satisfy the hypothesis above, all the points in Fig. 15 should lie in either the lower right quadrant (strong stretching & no growth) or the upper left quadrant (weak stretching & growth), with the dividing line at 1.

All but 4 points lie in these two quadrants. The majority of the plotted times the cyclones are growing in an environment of low stretching deformation. At 5 times [L_{R2} case (a), case (c) and 2 points from L_A case (d)] the cyclones are decaying in an environment of strong stretching deformation. There are 2 points in the lower right quadrant where the frontal cyclone has undergone a small decrease in amplitude, as measured by vorticity wavyness, however as illustrated in Fig. 13 [at 00GMT for L_U case (d)] this is only a small decrease in an overall growth period. There are also 2 points [from L_U case (d)] in the upper right quadrant. These are from 03GMT and 09GMT on the 21st January, early in the growth phase of L_U. It was noted that the stretching was falling at these times, but was still large, suggesting the idea that the *time rate-of-change of stretching may be important*, as well as the actual stretching rate. This should be a topic for future research.

In conclusion it appears the hypothesis relating barotropic frontal cyclone growth and environmental stretching is largely born out. The majority of data points fit the hypothesis with 4 exceptions. In dimensional units the theoretical critical threshold is in the range $0.5\text{-}1.2\text{x}10^{-5}\text{s}^{-1}$ for the analysed cases (taking $2\mu=0$, ie. an upper bound). For a typical strength vorticity front (an along-front average vorticity of about $1\text{x}10^{-4}\text{s}^{-1}$), a critical threshold around $0.8\text{x}10^{-5}\text{s}^{-1}$ seems to fit the observed results.

5. CONCLUSIONS

It has become clear that the role of stretching deformation, due to the synoptic environment of a front, is crucial in the evolution of any instabilities on that front. A change of stretching deformation over time, or location, can differentiate growth from suppression of frontal waves. For barotropic instabilities a hypothesis suggested by theoretical modelling work is largely born out - as summarised in Fig. 15. If the stretching deformation of the front is strong (relative to the vorticity strip), then barotropic instabilities are unlikely to grow. If the stretching deformation of the front is weak, then barotropic instabilities will be free to grow, in the form of edge waves on a low level potential vorticity strip if one exists. In certain cases the observed frontal wind derivatives were examined and compared to theoretical model perturbation wind derivatives, adding evidence that the frontal cyclone's growth was through barotropic edge wave amplification.

In addition, this study has provided a range of values for the commonly prescribed deformation frontogenesis parameter α, by calculating the environmental along-front stretching $\partial v_e/\partial y_f$. The calculated α ranged from $-0.5\times10^{-5}s^{-1}$ to $1.6\times10^{-5}s^{-1}$; the same order of magnitude as the standard theoretical value ($1.0\times10^{-5}s^{-1}$) but with a range that is significant for potential barotropic instability growth and indeed frontogenesis models. A two level extension of the attribution technique (see the Appendix) allowed the calculation of a range of values for the shearing frontogenesis parameter s^2 corresponding to -0.4K/100km to 0.1K/100km, slightly less than the values generally taken in frontogenesis studies.

The attribution technique developed here is based on the vorticity and divergence attribution of Bishop (1996I&II) and so is suited to phenomenon where 2 dimensional vorticity dynamics are important. For example when barotropic processes appear to play an important role, such as in secondary frontal cyclones or tropical cyclones. An interesting extension of the technique would be to examine vorticity on a (quasi-horizontal) isentropic surface. This would be appropriate for looking at upper tropospheric levels where flow is generally on isentropic surfaces. In this case isentropic vorticity is the key quantity, and this is equal to potential vorticity, scaled by a density factor. This variant would be useful in examining the stability of

upper tropospheric PV tongues and filaments, such as those seen in high resolution modelling studies (eg. Methven 1996) and on a broader scale in observed forecast model data (eg. Hoskins *et al.* 1985).

The operational forecasting of secondary frontal cyclones is of great importance and as discussed in the Introduction and found by this study, the evolving synoptic environment of the front is crucial for frontal cyclone development. Therefore the modification of the techniques outlined in this study into an operational forecasting tool to assess this synoptic environment is of the utmost priority, and is currently being pursued by the authors.

ACKNOWLEDGMENTS

The authors would like to thank Andy Macallan of the Joint Centre for Mesoscale Meteorology for assistance with obtaining the UK Met. Office data analysed in the study, and Raul Cunha at the University of Toronto for redrawing the pressure analyses. We would also like to thank Ted Shepherd, and two anonymous reviewers for helpful comments on the first draft of this paper. Ian Renfrew was funded by an NERC studentship during the course of this study which was completed at the University of Reading.

APPENDIX

Vorticity and divergence attribution can only be used on one level of data at one time, however without knowing the vertical structure of a front it is not possible to establish the amount of shear frontogenesis the front is undergoing. The classic Hoskins and Bretherton (1972) shear front has a prescribed *along-front* temperature gradient (equivalently a geostrophic vertical shear) given by the parameter $s^2 = -g/\theta_0 . \partial\theta/\partial y_f$. This cannot be estimated by a single level analysis, as if the temperature gradient is directly measured from observed data, local variations will mask the large scale value. Hence to measure s^2 accurately in real data the large scale induced along-front temperature gradient must be found. To do this a two-level attribution method is employed:

the attribution method is carried out for the 900mb and 700mb levels for example. Assuming a balance condition it is possible to retrieve the geopotential (ϕ) corresponding to a certain wind field. For example using geostrophic balance:

$$\phi = \frac{\psi}{f} \qquad (9)$$

where ψ is a streamfunction and f the Coriolis parameter (taken as constant). Differencing ϕ in the vertical via

$$\frac{\partial \phi}{\partial z} = \frac{g\theta}{\theta_0} = b \qquad (10)$$

(assuming hydrostatic balance) will yield the potential temperature field corresponding to that streamfunction. Unfortunately when the streamfunction is found at more than one level an arbitrary constant renders the actual value of the geopotential or potential temperature meaningless. However the main interests are the thermal gradients not the actual temperature itself, so differentiating in the horizontal:

$$\frac{\partial}{\partial y_f}\left(\frac{\partial \phi}{\partial z}\right) = -\frac{g}{\theta_0}\frac{\partial \theta}{\partial y_f} \quad \text{and} \quad \frac{\partial}{\partial x_f}\left(\frac{\partial \phi}{\partial z}\right) = \frac{g}{\theta_0}\frac{\partial \theta}{\partial x_f} \qquad (11)$$

the unknown constants are dispensed with, and the temperature gradients are retrieved. If the total streamfunction is used in the balance approximation (9) then the full temperature gradients are retrieved. If the streamfunction due to non-frontal vorticity (ψ_e) is used in (9), then the environmental along and across-front temperature gradients are retrieved, as in §3(b). So the prescribed values of s^2 in Hoskins and Bretherton (1972) or Keyser and Pecnick (1987) would be found. Note there are several approximations used in the above method:

- using only the streamfunction in the balance approximation means only considering the vorticity induced winds. The much smaller divergence induced winds are neglected. This is reasonable for a dominantly rotational flow.
- the simple geostrophic balance approximation $\phi=\psi/f$ is used as one would expect the

large scale flow to be in approximate geostrophic balance, so to find the large scale temperature gradients this balance is adequate. This is less justified in finding the frontal temperature gradients.

- hydrostatic balance is employed. This is a negligible approximation given the above.

Note the two-level method requires the fronts have a reasonably coherent vertical structure in vorticity. If cross-front thermal wind balance is maintained then this will be the case, and in most observed fronts this appears accurate (see Thorpe and Clough 1991 for example). The two level approximation can be used to calculate measures of deformation and shearing frontogenesis based on the environmental winds and frontal temperature gradients; and frontal winds and environmental temperature gradients respectively - see Renfrew (1995) for details.

REFERENCES

Ayrault, F., Lalaurette, F., Joly, A. and Loo, C. (1995): North Atlantic ultra high frequency variability: An introductory survey. *Tellus.* **47A**, 671-696.

Bell, R.S. (1994): The assimilation of ERS-1 scatterometer winds. *Forecasting Research Division Technical Report* , No. 89, Meteorological Office, Bracknell, UK.

Bishop, C.H. (1993I): On the behaviour of baroclinic waves undergoing horizontal deformation. I: The 'RT' phase diagram. *Q. J. R. Meteorol. Soc.* **119**, 221-240.

Bishop, C.H. (1993II): On the behaviour of baroclinic waves undergoing horizontal deformation. II: Error-bound amplification and Rossby wave diagnostics. *Q. J. R. Meteorol. Soc.* **119**, 241-267.

Bishop, C.H. (1996I): Domain independent attribution. I: Reconstructing the wind from estimates of vorticity and divergence using free space Greens functions. *J. Atmos. Sci.* **53**, 241-252.

Bishop, C.H. (1996II): Domain independent attribution. II: Its value in the verification of dynamical theories of frontal waves and frontogenesis. *J. Atmos. Sci.* **53**, 253-262.

Bishop, C.H. and Thorpe, A.J. (1994I): Frontal wave stability during moist deformation frontogenesis. Part I: Linear wave dynamics. *J. Atmos. Sci.* **51**, 852-873. *[BT94I]*

Bishop, C.H. and Thorpe, A.J. (1994II): Frontal wave stability during moist deformation frontogenesis. Part II: The suppression of nonlinear wave development. *J. Atmos. Sci.* **51**, 874-888. *[BT94II]*

Bishop, C.H. and Thorpe, A.J. (1994a): Potential vorticity and the electrostatics analogy: quasi-geostrophic theory. *Q. J. R. Meteorol. Soc.* **120**, 713-731.

Browning, K.A. and Roberts, N.M. (1994): Structure of a frontal cyclone. *Q. J. R. Meteorol. Soc.* **120**, 1535-1557.

Browning, K.A., Clough, S.A., Davitt, C.S.A., Roberts, N.M., Hewson, T.D. and Healy, P.G.W. (1995): Observations of the mesoscale substructure in the cold air of a developing frontal cyclone. *Q. J. R. Meteorol. Soc.* **121**, 1229-1254.

Charney, J.G. and Stern, M.E. (1962): On the stability of internal baroclinic jets in a rotating atmosphere. *J. Atmos. Sci.* **19**, 159-162.

Cullen, M. (1993): The unified forecast/climate model. *Meteorol. Mag.* **122**, 81-94.

Davis, C.A. (1992): Piecewise potential vorticity inversion. *J. Atmos. Sci.* **49**, 1397-1411.

Davis, C.A. and Emanuel, K.A. (1991): Potential vorticity diagnostics of cyclogenesis. *Mon. Wea. Rev.* **119**, 1929-1953.

Dritschel, D.G. (1989): On the stabilization of a two-dimensional vortex strip by adverse shear. *J. Fluid Mech.* **206,** 193-221.

Dritschel, D.G., Haynes, P.H., Juckes, M.N. and Shepherd, T.G. (1991): The stability of a two-dimensional vorticity filament under uniform strain. *J. Fluid Mech.* **230,** 647-665.

Hoskins, B.J. and Bretherton, F.P. (1972): Atmospheric frontogenesis models: Mathematical formulation and solution. *J. Atmos. Sci.* **29,** 11-37.

Hoskins, B.J., McIntyre, M.E. and Robertson, A.W. (1985): On the use and significance of isentropic potential vorticity maps. *Q. J. R. Meteorol. Soc.* **111,** 877-946.

Hoskins, B.J. and Berrisford, P. (1988): The storm of 15-16th October 1987: A potential vorticity perspective. *Weather,* **43,** 122-129.

Joly, A. (1995): The stability of steady fronts and the adjoint method: Nonmodal frontal waves. *J. Atmos. Sci.* **52,** 3082-3108.

Joly, A. and Thorpe, A.J. (1990): Frontal instability generated by tropospheric potential vorticity anomalies. *Q. J. R. Meteorol. Soc.* **116,** 525-560.

Joly, A. and Thorpe, A.J. (1991): The stability of time-dependent flows: An application to fronts in developing baroclinic waves. *J. Atmos. Sci.* **48,** 163-182.

Keyser, D. and Pecnick, M.J. (1987): The effect of along-front temperature variation in a two-dimensional primitive equation model of surface frontogenesis. *J. Atmos. Sci.* **44,** 577-604.

Lynch, P. (1988): Deducing the wind from vorticity and divergence. *Mon. Wea. Rev.* **116,** 86-93.

Lynch, P. (1989): Partitioning the wind in a limited domain. *Mon. Wea. Rev.* **117,** 1492-1500.

Malardel, S., Joly, A., Courbet, F. and Courtier, Ph. (1993): Nonlinear evolution of ordinary frontal waves induced by low-level potential vorticity anomalies. *Q. J. R. Meteorol. Soc.* **119,** 681-713.

Methven, J. (1996): Tracer behaviour in baroclinic waves. *PhD Thesis,* University of Reading.

Morse, P.M. and Feshbach, H. (1953): Methods of theoretical physics, *Vol. I and Vol. II,* McGraw-Hill Book Co. Ltd.

Parker, D.J. (1996): Barotropic instabilities in frontolytic strain. *(Submitted to Q. J. R. Meteorol. Soc.)*

Polavarapu, S.M. and Peltier, W.R. (1993): Formation of small-scale cyclones in numerical simulations of synoptic-scale baroclinic wave lifecycles: Secondary instabilities at the cusp. *J. Atmos. Sci.* **50,** 1047-1057.

Renfrew, I.A. (1995): The development of secondary frontal cyclones. *PhD Thesis,* University of Reading.

Schär, Ch. and Davies, H.C. (1990): An instability of mature cold fronts. *J. Atmos. Sci.* **47,** 929-950.

Thorncroft, C.D. and Hoskins, B.J. (1990): Frontal cyclogenesis. *J. Atmos. Sci.* **47,** 2317-2336.

Thorpe, A.J. and Clough, S. (1991): Mesoscale dynamics of cold fronts: structures described by dropsoundings in FRONTS 87. *Q. J. R. Meteorol. Soc.* **117,** 903-941.

FIGURE CAPTIONS

Figure 1 Mean-sea-level pressure map at 12GMT on the 12th November 1994 for the North Atlantic sector - redrawn from the UK Met. Office manual analysis. Isobars are every 4mb and lines of latitude & longtitude are every 10°. The frontal cyclone (L_{R1}) is indicated on the cold front of parent cyclone L_R.

Figure 2 A schematic of a frontal box defined for a synoptic low.

Figure 3 Relative vorticity plots at **(a)** 00GMT and **(b)** 12GMT on the 12th November 1994 and **(c)** 00GMT on the 13th, at the 900mb level. Parts (a) and (b) show L_{R1} in the frontal box (outlined in bold) and part (c) shows L_{R1} and L_{R2}. The contour interval is $0.4 \times 10^{-4} s^{-1}$, with lines of latitude & longtitude drawn every 10° and the axes labelled in km.

Figure 4 Contours of along-front stretching for **(a)** the observed winds, and **(b)** the environmental winds, at 00GMT on the 12th November 1994, for the frontal box indicated in Fig. 3(a). Also shown are vectors of the corresponding winds ie. $\boldsymbol{u}_{obs}$ and $\boldsymbol{u}_e$ respectively. The contour interval is $0.5 \times 10^{-5} s^{-1}$ and the scaling arrows for the winds are $28 ms^{-1}$. The axes labelling is in km.

Figure 5 Vorticity wavyness $W(\xi)$ and the maximum along-front averaged vorticity for the 30 hour period of investigation of L_{R1} and L_{R2} of case (a). The along-front averaged vorticity is over the full frontal box.

Figure 6 Along-front environmental stretching rates at the 900mb and 700mb levels for L_{R1} and L_{R2} of case (a). The plotted values are averages over the central half of the frontal box.

Figure 7 Contours of the along-front frontal-induced wind derivatives $\partial v_f/\partial y_f$ **(left)** at 12GMT & 18GMT, and $\partial u_f/\partial y_f$ **(right)** at 12GMT & 18GMT on 12th November 1994. The vectors are the corresponding $\boldsymbol{u}_f$ winds. The contour interval is $1\times10^{-5}s^{-1}$ the same as Fig. 10 in *BT94II*. The scaling arrow is $15ms^{-1}$. The frontal box for 12GMT is as shown in Fig. 3(b).

Figure 8 Mean-sea-level pressure map at 18GMT on the 1st February 1994 for the North Atlantic sector - redrawn from the UK Met. Office manual analysis. Isobars are every 4mb. Frontal cyclones L_Q and L_R are analysed with closed isobars at this time.

Figure 9 A cross-section of potential vorticity (shading) and isentropes (contours) along the elongated front, passing through L_R (left) and L_Q (right) at 12GMT on the 2nd February. The shading indicates PV values at an interval of 0.2 PVU from -0.2 to 1.6; the isentropes are every 5K as labelled.

Figure 10 Mean-sea-level pressure map at 00GMT on the 26th November 1994 - redrawn from the UK Met. Office manual analysis. Isobars are every 4mb. The cold front of L_L that is examined is labelled 'M' and 'N'.

Figure 11 Relative vorticity at 900mb for 00GMT on the 26th November 1994. As in Fig. 3 the frontal box is outlined in bold, and the contour interval is $0.4\times10^{-4}s^{-1}$.

Figure 12 Mean-sea-level pressure analysis for 18GMT on the 21st January 1995 - redrawn from the UK Met. Office manual analysis. Isobars are every 4mb. Frontal cyclone L_A, now a parent cyclone, and L_U a col wave on its cold front are labelled.

Figure 13 Vorticity wavyness $W(\xi)$ and the maximum along-front averaged vorticity for the 60 hour period of investigation of L_A and L_U of case (d). The along-front average is taken over individual frontal boxes for each cyclone.

Figure 14 Along-front environmental stretching rates at 900mb for L_A and L_U of case (d). The plotted values are averages over the central half of the frontal box.

Figure 15 A regime diagram showing growth against along-front stretching. The growth is measured as the rate of change of vorticity wavyness $W(\xi)$ (units $x10^{-9}s^{-2}$) and the stretching is measured as $\partial v_e/\partial y_f$ normalised by α_{min} (the critical threshold for suppression of all barotropic waves). Data points are plotted for all four cases. The error bars indicate the maximum errors found in the sensitivity study of case (a), as mentioned in section 2. In the upper right quadrant waves are growing in weak environmental stretching deformation; in the lower left quadrant wave growth is suppressed by the strong environmental stretching deformation.

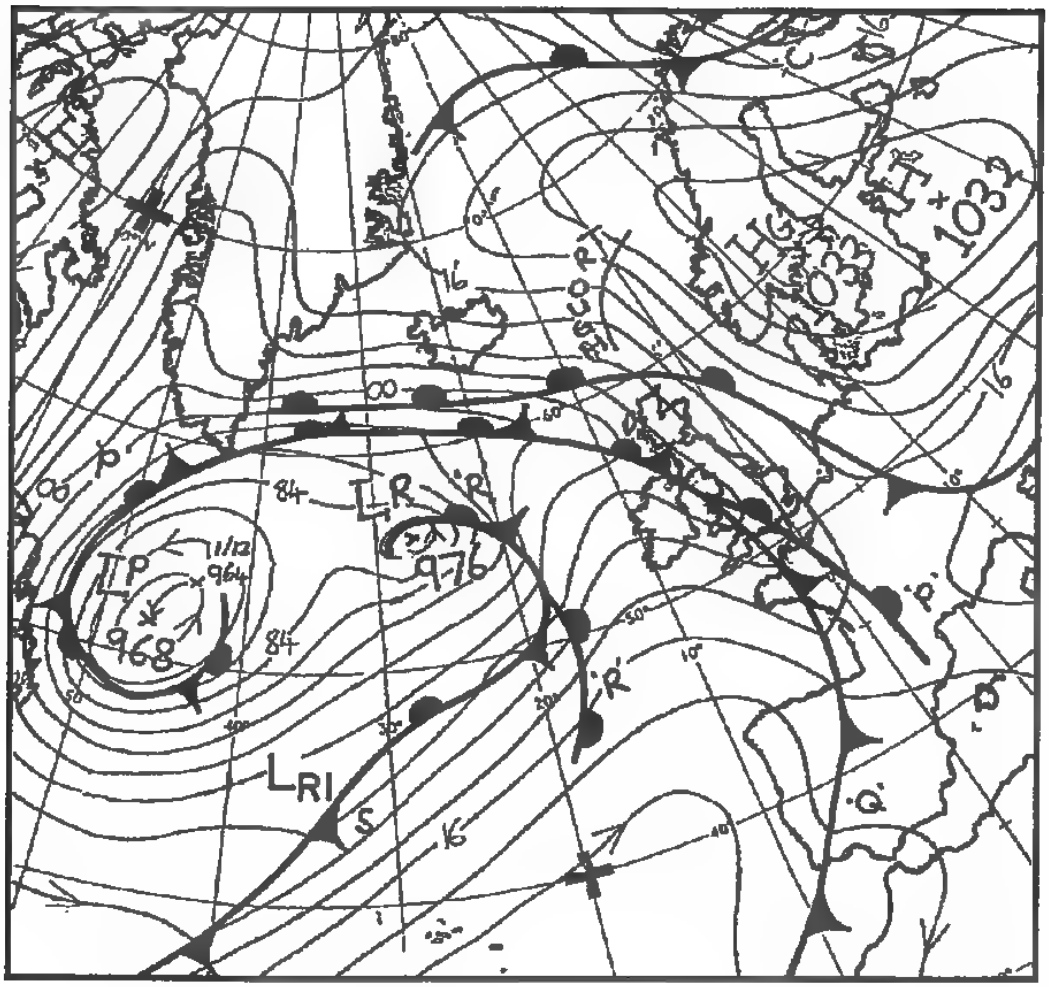

LP
968
964
976
LR
LRI
84
16
1033

2

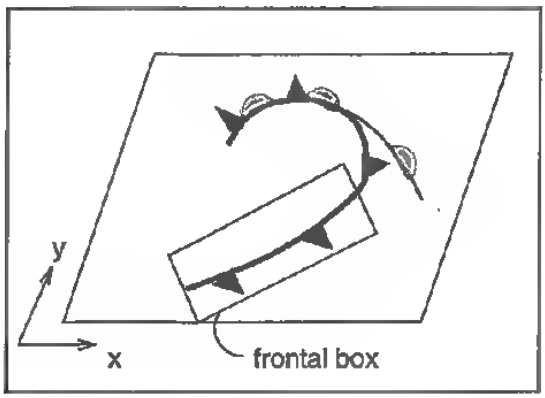

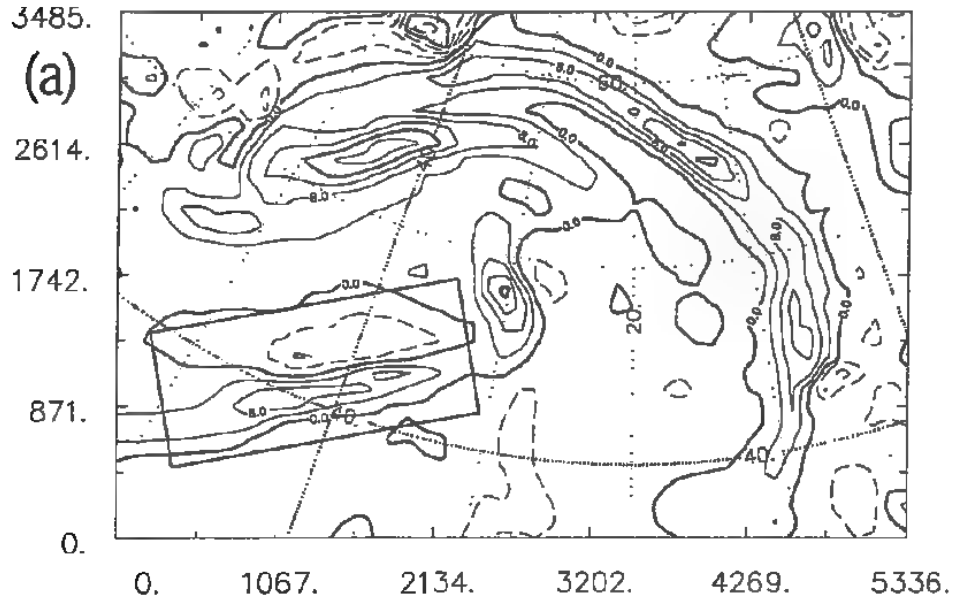
3485.
(a)
2614.
1742.
871.
0.
0.
1067.
2134.
3202.
4269.
5336.

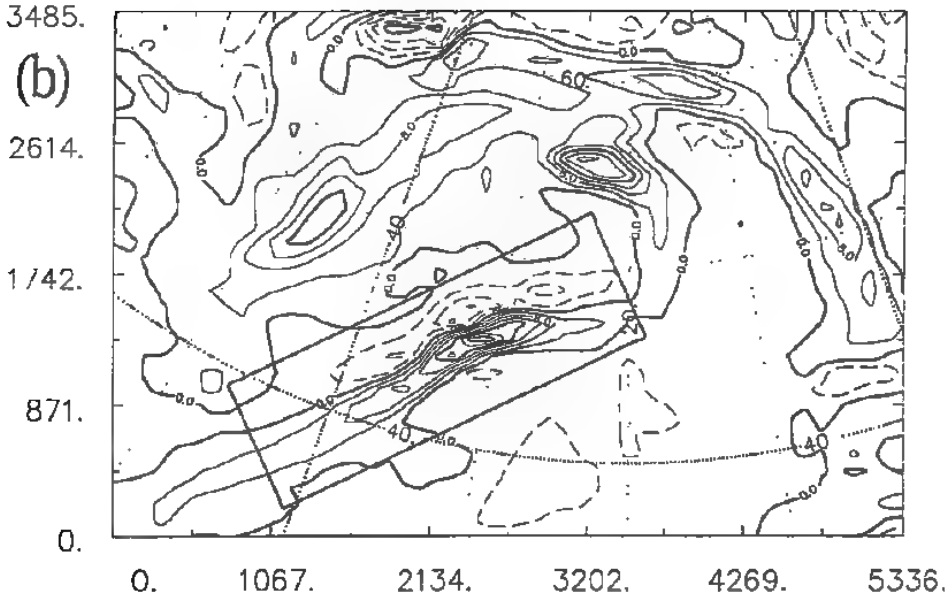
3485.
(b)
2614.
1742.
871.
0.
0.
1067.
2134.
3202.
4269.
5336.

3

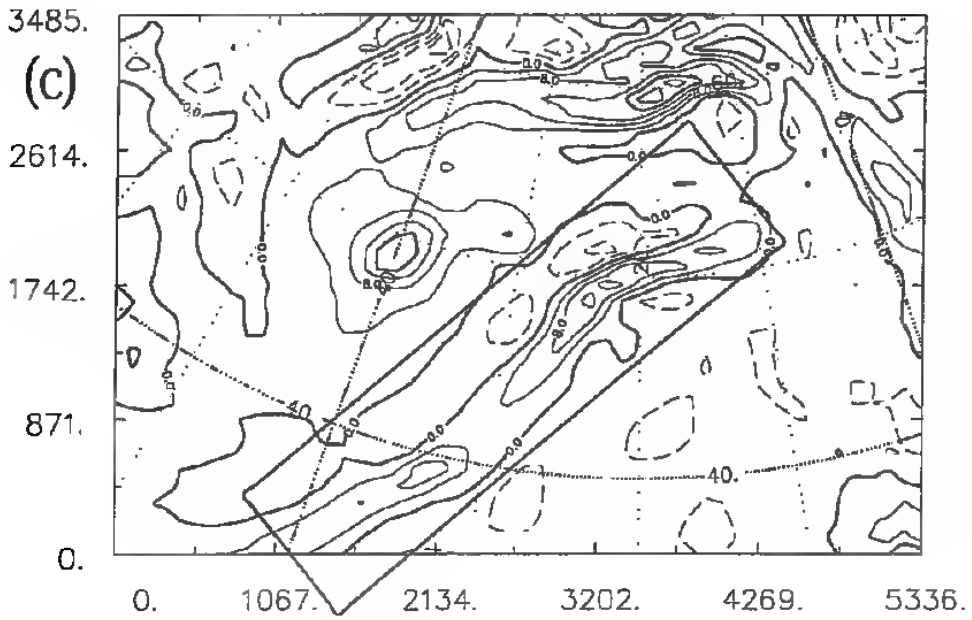

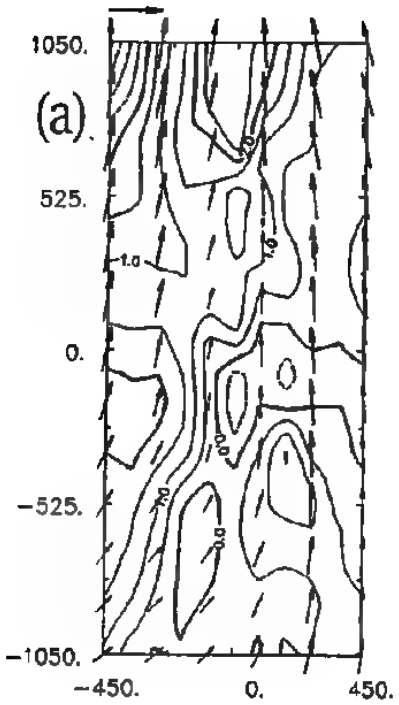
(a)
1050.
525.
0.
−525.
−1050.
−450.
0.
450.
1.0
1.0
1.0
1.0
1.0

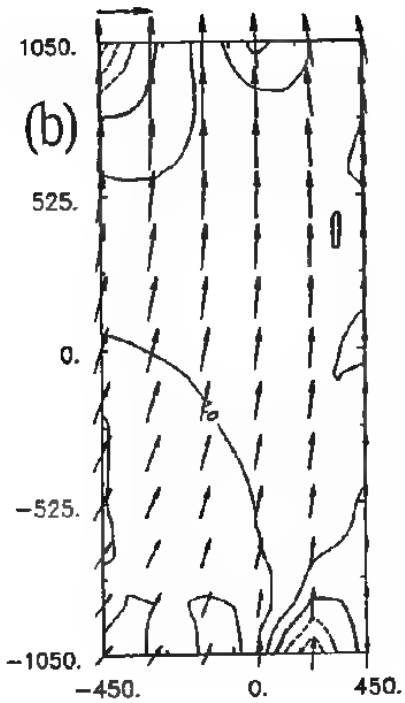
(b)
1050.
525.
0.
−525.
−1050.
−450.
0.
450.

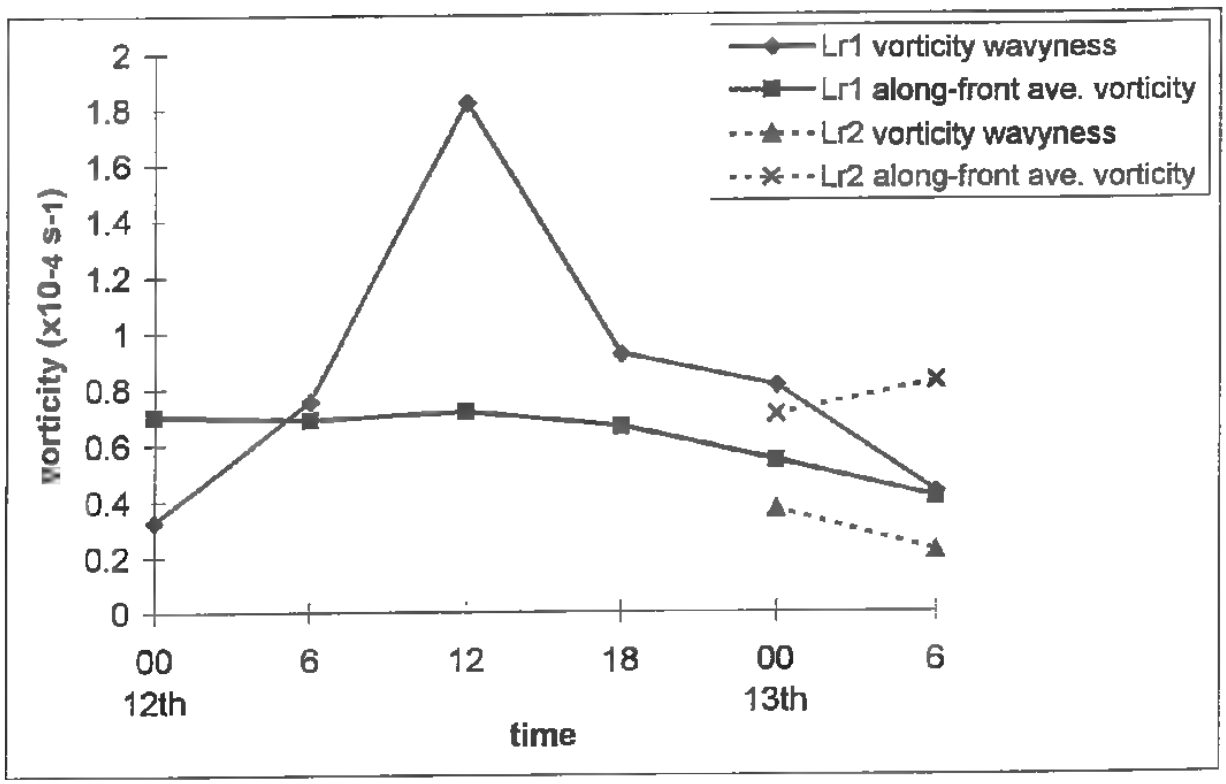
Lr1 vorticity wavyness
Lr1 along-front ave. vorticity
Lr2 vorticity wavyness
Lr2 along-front ave. vorticity
vorticity (x10-4 s-1)
2
1.8
1.6
1.4
1.2
1
0.8
0.6
0.4
0.2
0
00
12th
6
12
18
00
13th
6
time

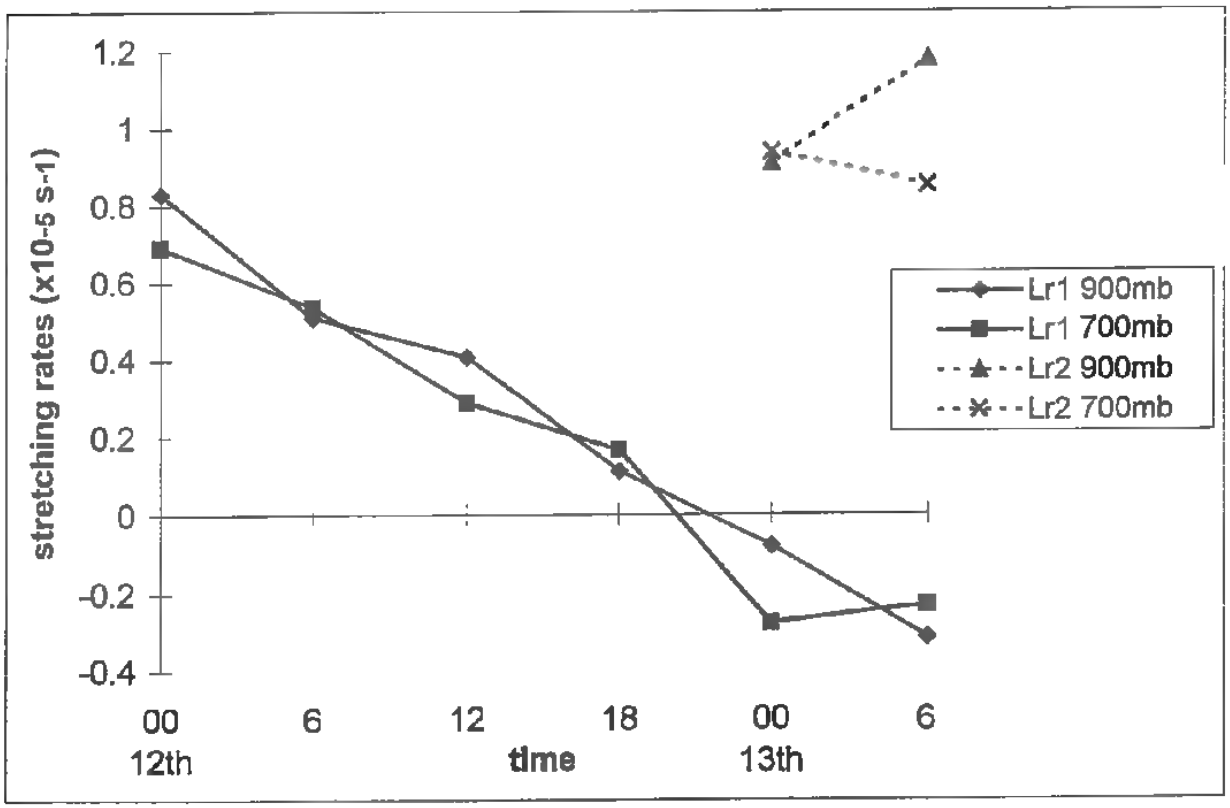
Lr1 900mb
Lr1 700mb
Lr2 900mb
Lr2 700mb
stretching rates (x10-5 s-1)
1.2
1
0.8
0.6
0.4
0.2
0
-0.2
-0.4
00
12th
6
12
18
00
13th
6
time

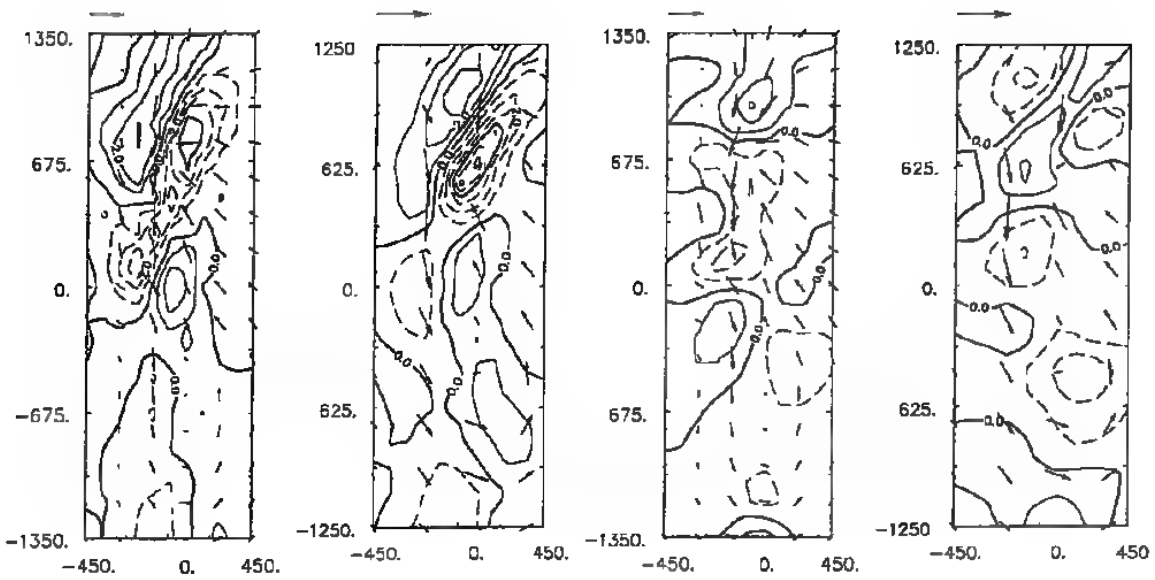
1350.
675.
0.
-675.
-1350.
-450.
0.
450.
1250
625.
0.
625.
-1250.
-450.
0.
450.
1350.
675.
0.
675.
-1350.
-450.
0.
450.
1250.
625.
0.
625.
-1250
-450.
0.
450

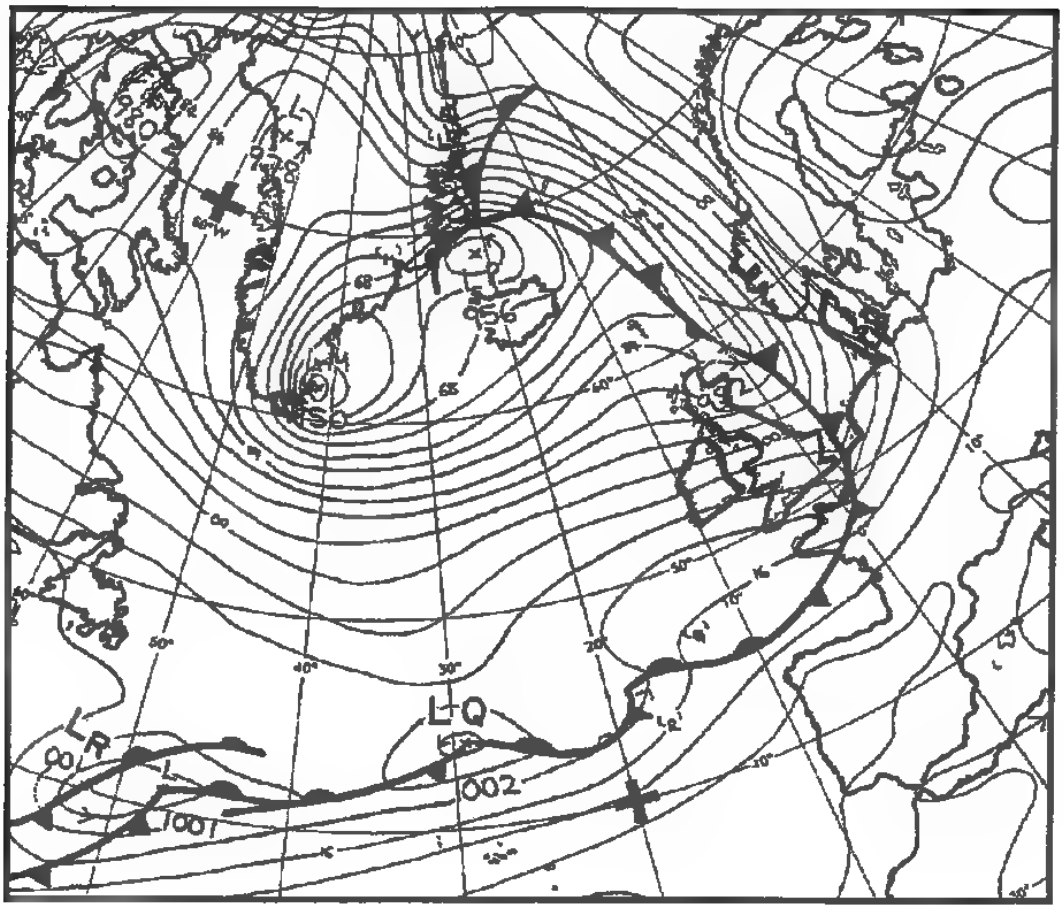
L
Q
1001
002

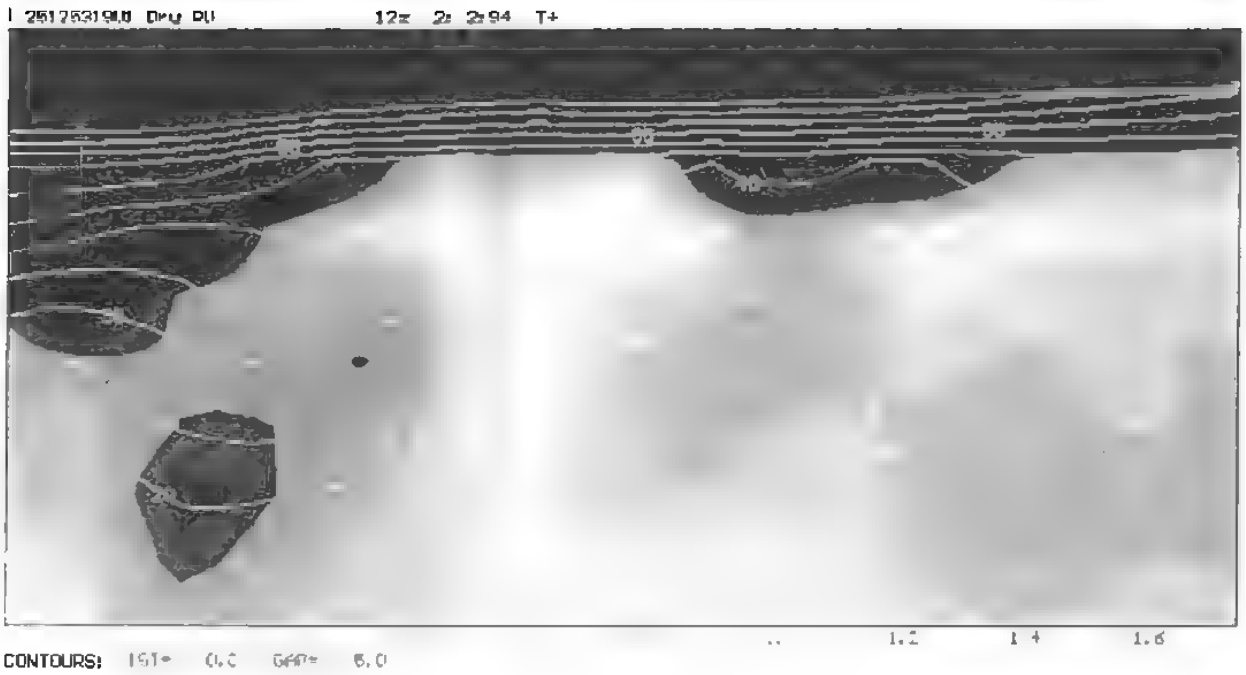
12z 2: 2:94 T+
1.2
1.4
1.6
CONTOURS:

0

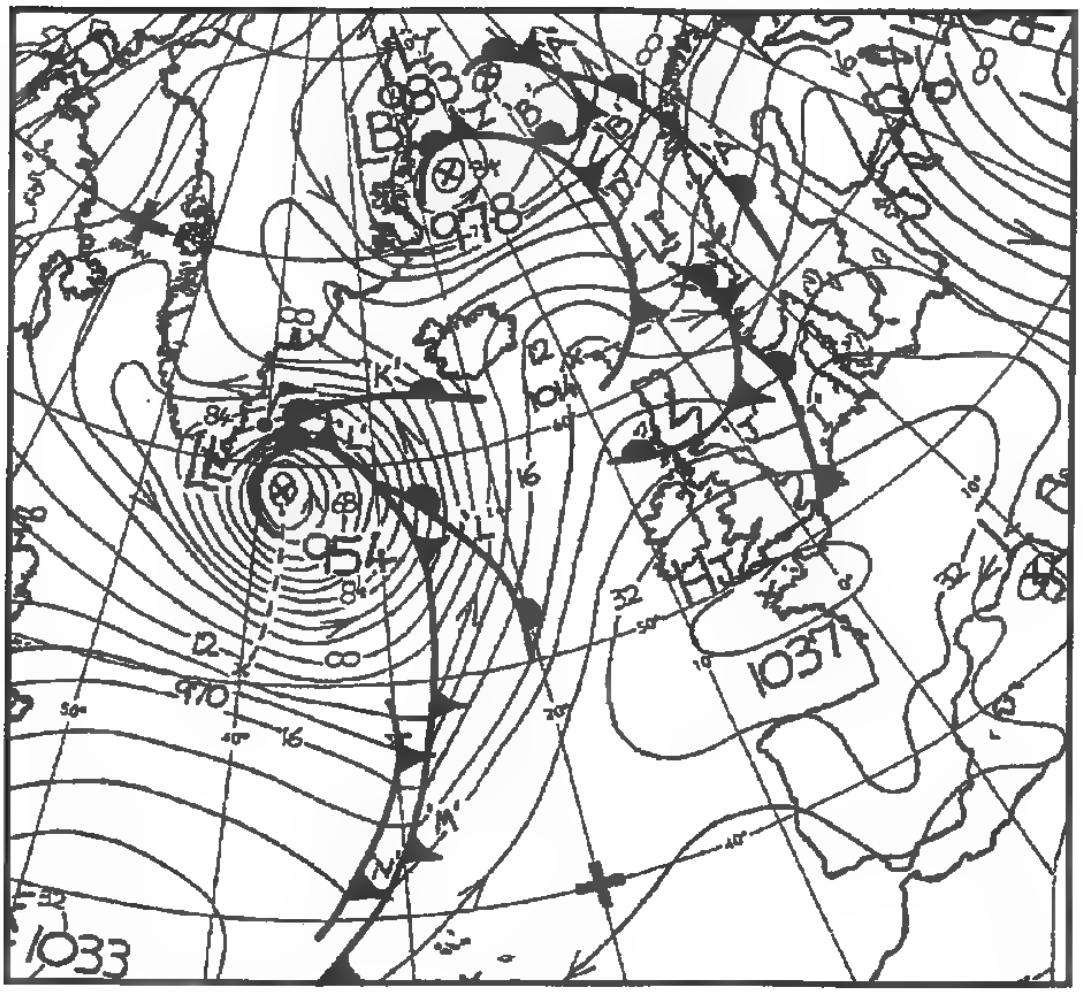

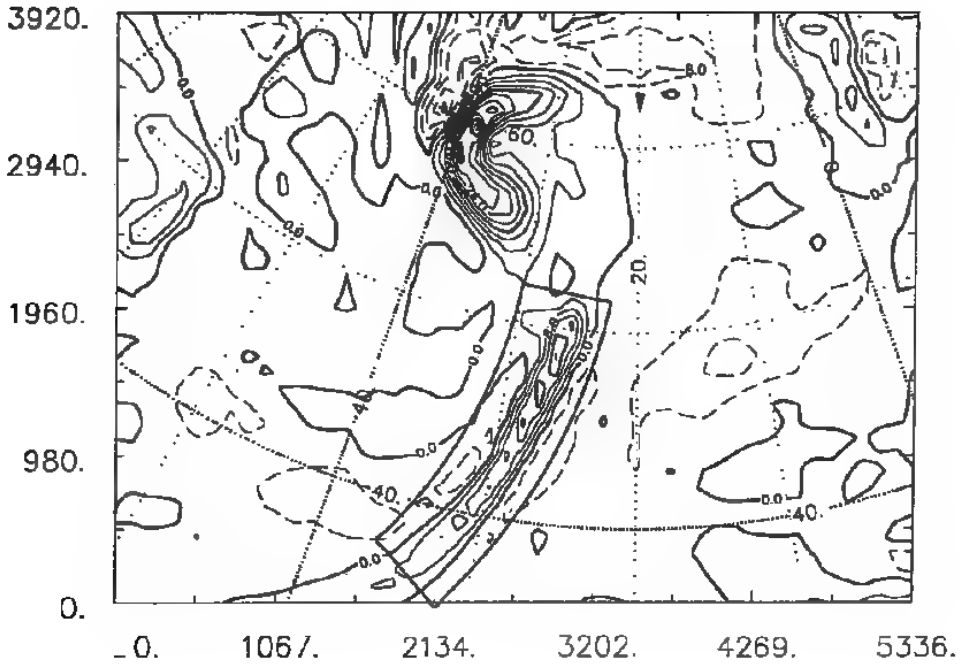
3920.
2940.
1960.
980.
0.
0.
1067.
2134.
3202.
4269.
5336.
60.
40.
20.
0.0

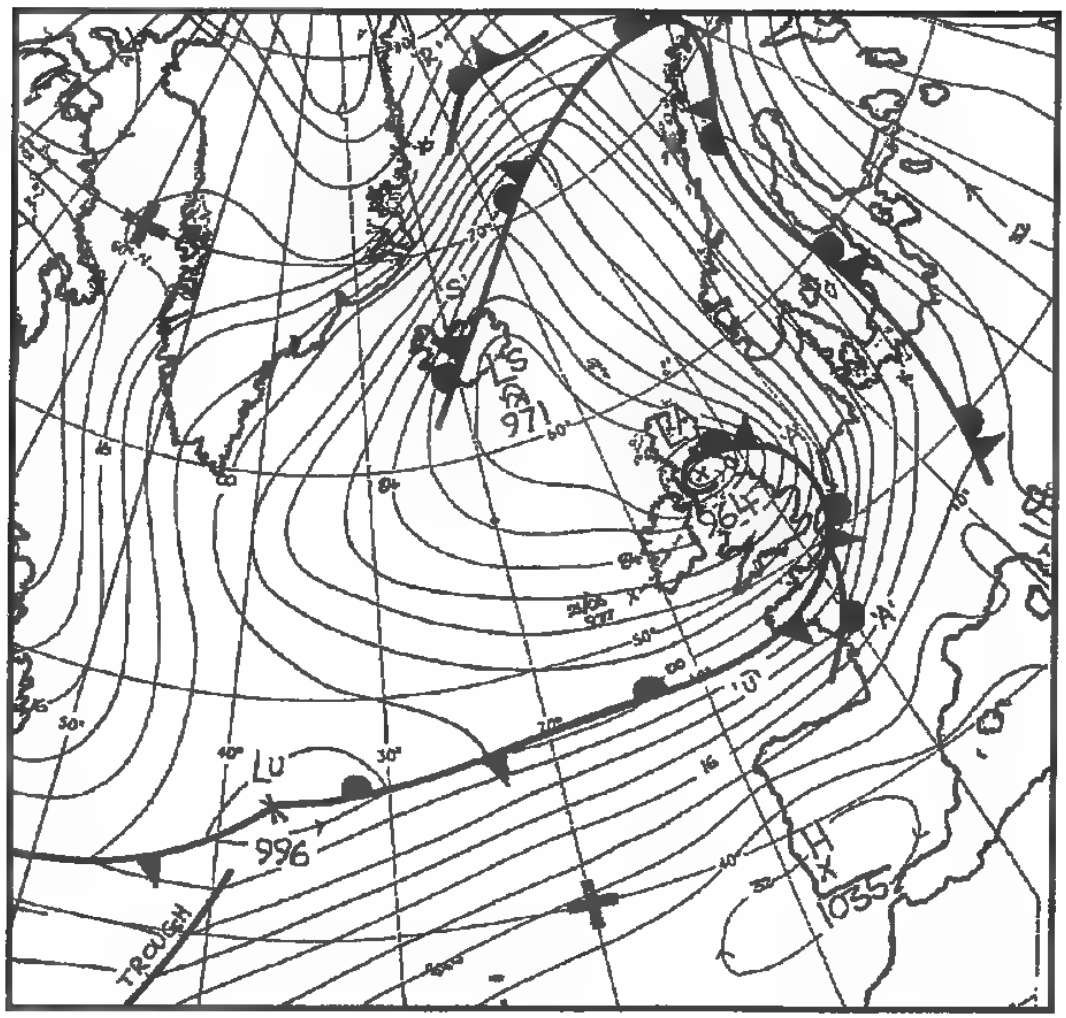

LS
971
964
LU
996
H
1035
TROUGH

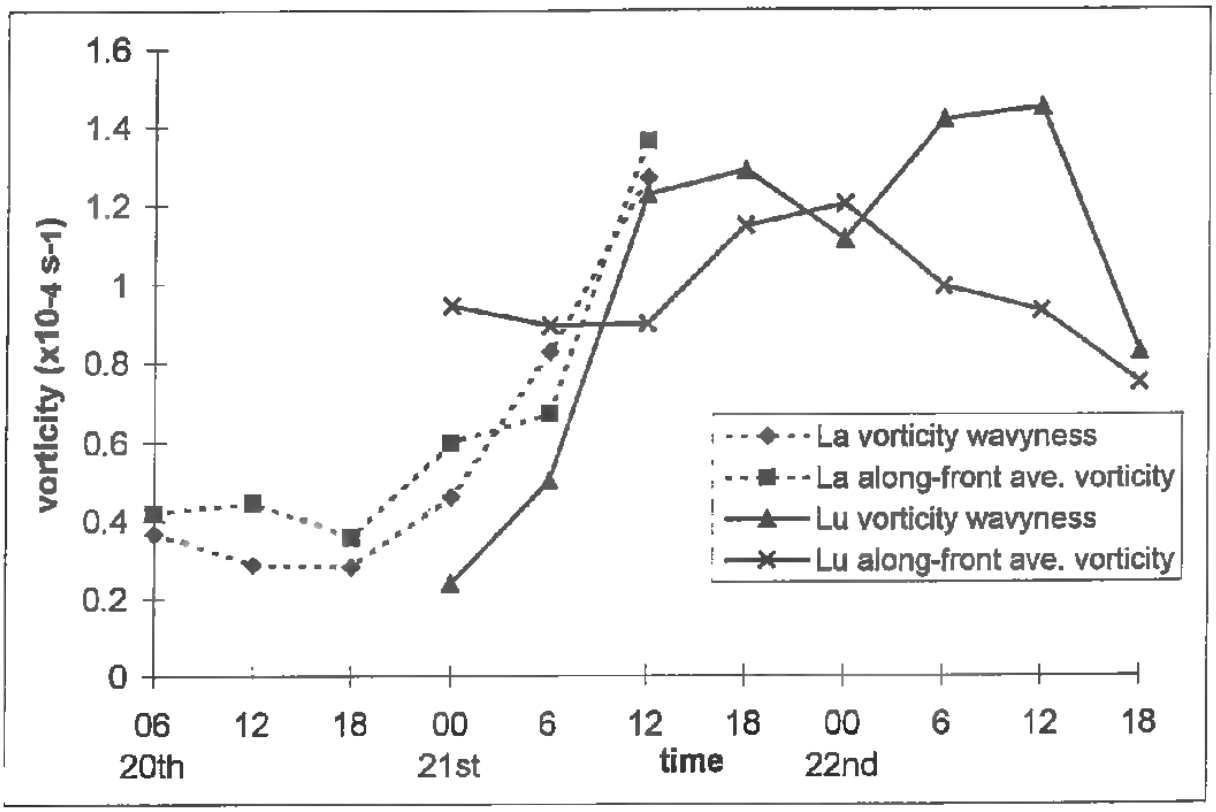
1.6
1.4
1.2
1
0.8
0.6
0.4
0.2
0
vorticity (x10-4 s-1)
La vorticity wavyness
La along-front ave. vorticity
Lu vorticity wavyness
Lu along-front ave. vorticity
06
12
18
00
6
12
18
00
6
12
18
20th
21st
time
22nd

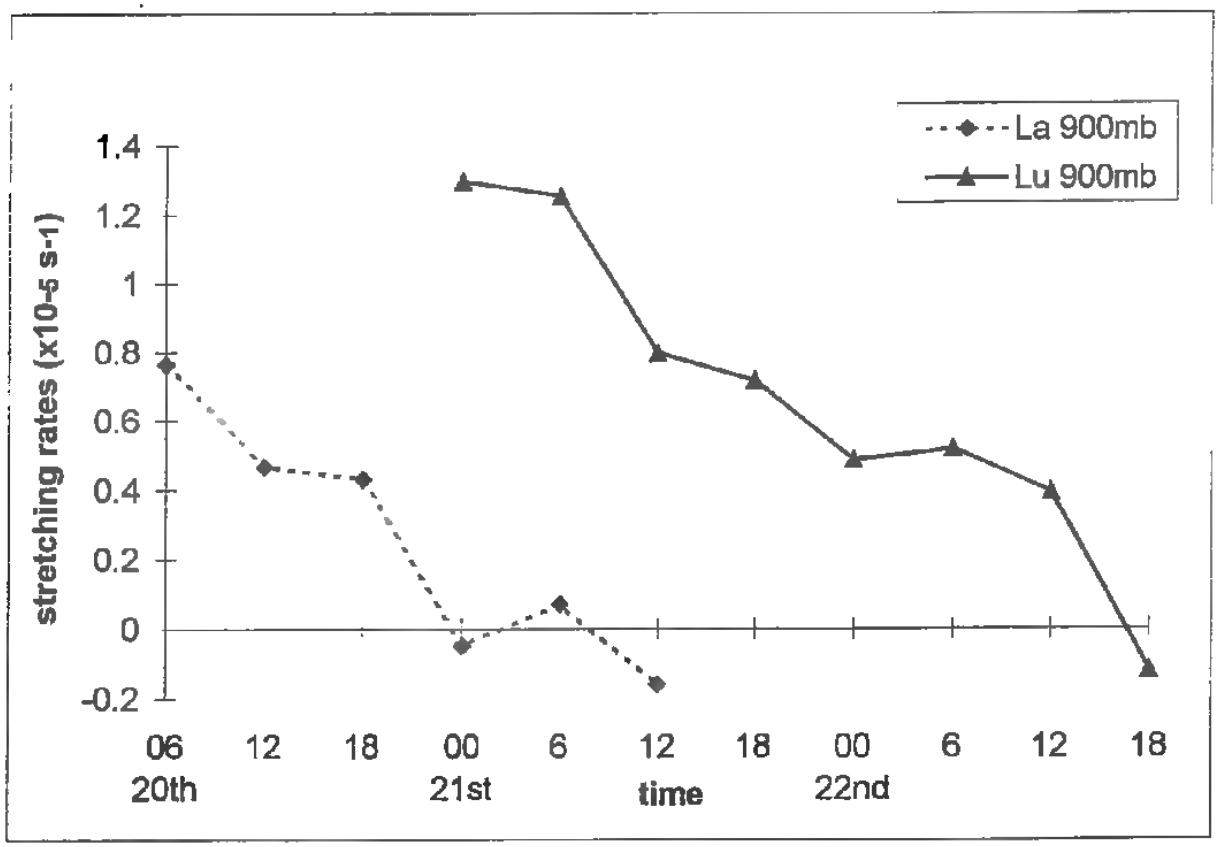
1.4
1.2
1
0.8
0.6
0.4
0.2
0
-0.2
stretching rates (x10-5 s-1)
La 900mb
Lu 900mb
06
12
18
00
6
12
18
00
6
12
18
20th
21st
time
22nd

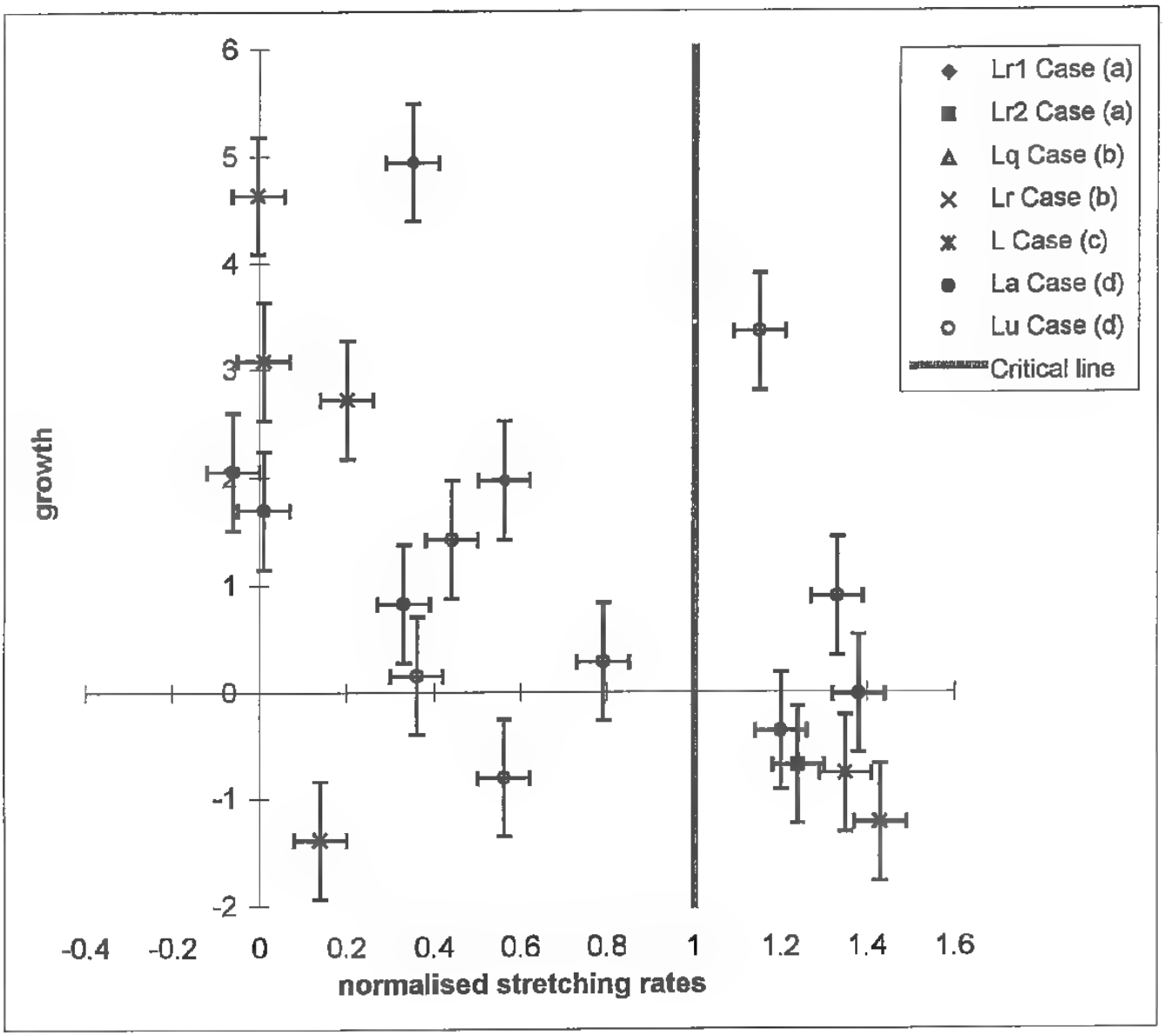
Lr1 Case (a)
Lr2 Case (a)
Lq Case (b)
Lr Case (b)
L Case (c)
La Case (d)
Lu Case (d)
Critical line
growth
normalised stretching rates
6
5
4
3
2
1
0
-1
-2
-0.4
-0.2
0
0.2
0.4
0.6
0.8
1
1.2
1.4
1.6

CURRENT JCMM INTERNAL REPORTS

This series of JCMM Internal Reports, initiated in 1993, contains unpublished reports and also versions of articles submitted for publication. The complete set of Internal Reports is available from the National Meteorological Library on loan, if required.

1. **Research Strategy and Programme**
   K A Browning et al
   January 1993

2. **The GEWEX Cloud System Study (GCSS)**
   GEWEX Cloud System Science Team
   January 1993

3. **Evolution of a mesoscale upper tropospheric vorticity maximum and comma cloud from a cloud-free two dimensional potential vorticity anomaly**
   K A Browning
   January 1993

4. **The Global Energy and Water Cycle**
   K A Browning
   July 1993

5. **Structure of a midlatitude cyclone before occlusion**
   K A Browning and N Roberts
   July 1993

6. **Development in Systems and Tools for Weather Forecasting**
   K A Browning and G Szejwach
   July 1993

7. **Diagnostic study of a narrow cold frontal rainband and severe winds associated with a stratospheric intrusion**
   K A Browning and R Reynolds
   August 1993

8. **Survey of perceived priority issues in the parametrizations of cloud-related processes in GCMs**
   K A Browning
   September 1993

9. **The Effect of Rain on Longwave Radiation**
   I Dharssi
   September 1993

10. **Physical Cloud Microprocesses - A Description of the Parametrization used in the Large Eddy Model**
H Swann
July 1994

11. **An Appreciation of the Meteorological Research of Ernst Kleinschmidt**
A J Thorpe
May 1992

12. **Potential Vorticity of Flow Along the Alps**
A J Thorpe, H Volkert and Dietrich Heimann
August 1992

13. **The Representation of Fronts**
A J Thorpe
January 1993

14. **A Parametrization Scheme for Symmetric Instability: Test for an Idealised Flow**
C S Chan and A J Thorpe
February 1993

15. **The Fronts 92 Experiment: a Quicklook Atlas**
Edited by T D Hewson
November 1993

16. **Frontal wave stability during moist deformation frontogenesis**
Part 1. Linear wave dynamics
C H Bishop and A J Thorpe
May 1993

17. **Frontal wave stability during moist deformation frontogenesis**
Part 2. The suppression of non-linear wave development
C H Bishop and A J Thorpe
May 1993

18. **Gravity waves in sheared ducts**
C Bishop and A J Thorpe
November 1993

19. **Potential Vorticity and the Electrostatics Analogy: Quasi - Geostrophic Theory**
C Bishop and A J Thorpe
November 1993

20. **Recent Advances in the Measurement of Precipitation by Radar**
A J Illingworth - April 1993

21. **Micro-Physique et Givrage. Cloud Microphysics and Aircraft Icing**
A J Illingworth May 1993

22. **Differential Phase Measurements of Precipitation**
M Blackman and A J Illingworth
May 1993

23. **Estimation of Effective Radius of Cloud Particles from the Radar Reflectivity**
N I Fox and A J Illingworth
May 1993

24. **A Simple Method of Dopplerising a Pulsed Magnetron Radar**
A Hau, A J Illingworth and J Eastment
November 1993

25. **Radiation and Polar Lows**
George C Craig
February 1994

26. **Collected preprints submitted to the International Symposium on the Life Cycles of Extratropical Cyclones; Bergen, Norway, 27 June - 1 July 1994**
April 1994

27. **Convective Frontogenesis**
Douglas J Parker and Alan J Thorpe
April 1994

28. **Improved Measurement of the Ice Water Content in Cirrus Using a Total Water Evaporator**
Philip R A Brown and Peter N Francis
April 1994

29. **Mesoscale Effects of a Dry Intrusion within a Vigorous Cyclone**
K A Browning and B W Golding
April 1994

30. **GEWEX Cloud System Study, Science Plan**
May 1994

31. **Parametrization of Momentum Transport by Convectively Generated Gravity Waves**
R Kershaw
February 1995

32. **Mesoscale Modelling Newsletter No 5**
May 1994

33. **Observations of the mesoscale sub-structure in the cold air of a developing frontal cyclone**
K A Browning, S A Clough, C S A Davitt, N M Roberts and T D Hewson
May 1994

34. **Longwave Radiative Forcing of a Simulated Tropical Squall Line**
Imtiaz Dharssi
July 1994

35. **On the nature of the convective circulation at a kata-cold front**
K A Browning
September 1994

36. **Collective preprints of papers submitted to the COST-75 International Seminar on Advanced Weather Radar Systems, Brussels, 20-23 September 1994**
November 1994

37. **Use of satellite imagery to diagnose events leading to frontal thunderstorms: Parts 1 and 11 of a case study**
K A Browning and N M Roberts
November 1994

38. **The role of spaceborne millimetre-wave radar in the global monitoring of ice cloud**
P R A Brown, A J Illingworth, A J Heymsfield, G M McFarquahar, K A Browning and M Gosset
December 1994

39. **Potential Vorticity Inversion**
Michael Ziemianski
October 1994

40. **Theory of mature tropical cyclones; a comparison between Kleinschmidt (1951) and Emanuel (1986)**
Suzanne L Gray
December 1994

41. **Dispersion and removal of pollutants during the passage of an atmospheric frontal System**
N R Gimson
December 1994

42. **The role of snow sublimation in frontogenesis**
D J Parker and A J Thorpe
December 1994

43. **Potential vorticity and the electrostatics Analogy: Ertel- Rossby formulation**
A J Thorpe and C H Bishop
December 1994

44. **Mesoscale aspect of extratropical cyclones: an observational perspective**
K A Browning
January 1995

45. **A Polar Low Outbreak: Evolution and Mesoscale Structures**
T D Hewson, G C Craig and C Claud
February 1995

46. **Generation of near-surface gusts of deep convection**
K Nakamura and R Kershaw
April 1995

47. **Attribution Concepts applied to the Omega Equation**
S A Clough, C S A Davitt and A J Thorpe
June 1995

48. **Parametrization of mixed-phase cloud and precipitation**
Susan P Ballard and M Gerard Hutchinson
June 1995

49. **Short-range forecasting of stratocumulus: Initialization Prediction**
Susan Ballard, Simon D Jackson and B Macpherson
June 1995

50. **Contributions of the JCMM/Dept of Meteorology Radar Group to the 27th AMS Radar Meteorology Conference, Vail October 1995**
June 1995

51. **Cold Pools in Shear**
Douglas J Parker
September 1995

52. **High-resolution analysis of frontal fracture**
K A Browning, S P Ballard and C S A Davitt
September 1995

53. **The Albedo of Broken Cloud Fields: Calculations using a modified two stream radiation code**
Imtiaz Dharssi and Roy Kershaw
October 1995

54. **Parametrization of momentum transport by convection. I: Theory and cloud modelling results**
P Kershaw and D Gregory
November 1995

55. **Variation of frontal structure along a cold front**
K A Browning and N M Roberts
November 1995

56. **Secondary Frontal Waves**
Douglas Parker
December 1995

57. **Objective Fronts**
T D Hewson
March 1996

58. **Mesoscale analysis of the activation of a cold front during cyclogenesis**
K A Browning, N M Roberts and A J Illingworth
June 1996

59. **Investigation of Different Representations of Rain in a 1-d Evaporation Model**
H Swann
May 1996

60. **Parametrization of diabatic processes in the inversion of the omega-equation**
M Athanassiadou and A J Thorpe

61. **The Role of the Environmental Flow in the Development of Secondary Frontal Cyclones**
I A Renfrew, A J Thorpe and A Joly
June 1996

62. **Consequences of the geostrophic momentum approximation on barotropic instability**
S Malardel, A J Thorpe and A Joly
June 1996

63. **Contributions to the AMS/RMS Conference on Mesoscale Processes**
Reading, 9-13 September 1996

64. **Vorticity and Potential Vorticity in Stratified Flows Interacting with an Isolated Obstacle**
Jorge A Gutierrez and A J Thorpe
September 1996

65. **Triple Point Development: Two Case Studies**
Douglas Parker
September 1996

66. **Radar observations of wind-shear splitting within evolving atmospheric Kelvin-Helmholtz billows**
D Chapman and K A Browning
April 1997

67. **Cold Frontal Structure derived from radar wind profilers**
K A Browning, D Jerrett, J Nash, T Oakley, N M Roberts
May 1997

68. **The dry intrusion and its effect on the frontal, cloud and precipitation structure of extratropical cyclones**
K A Browning - Text of invited special lecture at the Spring Conference of the Meteorological Society of Japan, University of Tsukuba, 22 May 1997

69. **Met. Office Unified Model data, diagnostic graphics programs, and other observational data available from the JCMM through the aegis of the Universities Weather Research Network UWERN.** Plus supplement.
Peter Panagi and Ed Dicks
June 1997

70. **Contributions of the JCMM/Dept of Meteorology Radar Group to 28th AMS Radar Meteorology Conference.** Austin, Texas, September 1997

71. **Sensitivity of short-range weather forecasts to local potential vorticity modifications**
Meral Demirtas and Alan Thorpe
July 1997

72. **Objective identification of frontal wave cyclones**
T D Hewson
August 1997

73. **Attribution and its application to mesoscale structure associated with tropopause folds**
A J Thorpe
September 1997

74. **The Role of the Environmental Flow in the Development of Secondary Frontal Cyclones**
Ian A Renfrew, Alan J Thorpe and Craig H Bishop
September 1997

Met Office Joint Centre for Mesoscale Meteorology Department of Meteorology
University of Reading PO Box 243 Reading RG6 6BB United Kingdom
Tel: +44 (0)118 931 8425 Fax: +44 (0)118 931 8791
www.metoffice.com